Article

Development of a Composite Hydrogel Containing Statistically Optimized PDGF-Loaded Polymeric Nanospheres for Skin Regeneration: In Vitro Evaluation and Stem Cell Differentiation Studies

Raheleh Hazrati, Effat Alizadeh,* Somaieh Soltani, Peyman Keyhanvar, and Soodabeh Davaran*

Read Online

ACCESS | Metrics & More | Article Recommendations

ABSTRACT: Platelet-derived growth factor-BB (PDGF-BB) is a polypeptide growth factor generated by platelet granules faced to cytokines. It plays a role in forming and remodeling various tissue types, including epithelial tissue, through interaction with cell-surface receptors on most mesenchymal origin cells. However, it breaks down quickly in biological fluids, emphasizing the importance of preserving them from biodegradation. To address this challenge, we formulated and evaluated PDGF-encapsulated nanospheres (PD@PCEC) using polycaprolactone-polyethylene glycol-polycaprolactone. PD@PCECs were fabricated through the triple emulsion methodology and optimized by using the Box–Behnken design. The encapsulation efficiency (EE) of nanoencapsulated PDGF-BB was investigated concerning four variables: stirring rate (X_1), stirring duration (X_2), poly(vinyl alcohol) concentration (X_3), and PDGF-BB concentration (X_4). The selected optimized nanospheres were integrated into a gelatin-collagen scaffold (PD@PCEC@GC) and assessed for morphology, biocompatibility, in vitro release, and differentiation-inducing activity in human adipose-derived stem cells (hADSCs). The optimized PD@PCEC nanospheres exhibited a particle size of 177.9 ± 91 nm, a zeta potential of 5.2 mV, and an EE of 87.7 ± 0.44%. The release profile demonstrated approximately 85% of loaded PDGF-BB released during the first 360 h, with a sustained release over the entire 504 h period, maintaining bioactivity of 87.3%. The study also included an evaluation of the physicochemical properties of the scaffolds and an assessment of hADSC adhesion to the scaffold's surface. Additionally, hADSCs cultivated within the scaffold effectively differentiated into keratinocyte-like cells (KLCs) over 21 days, evidenced by morphological changes and upregulation of keratinocyte-specific genes, including cytokeratin 18, cytokeratin 19, and involucrin, at both transcriptional and protein levels.
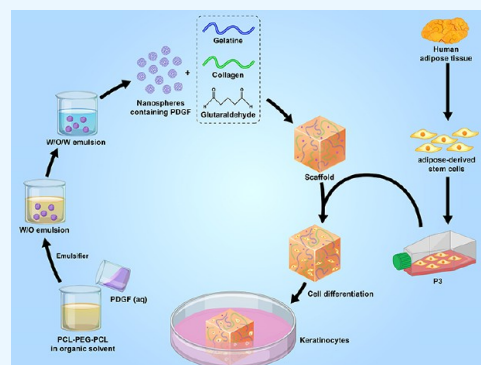
1. INTRODUCTION

Fast and appropriate wound healing is critical in treating severe burns, trauma, diabetic wounds, bedsores, and similar cases. The limited self-healing capacity of chronic wounds and extensive skin injuries poses a significant challenge to clinical practice. Despite their effectiveness for superficial wounds, conventional wound healing techniques often fail to support the regeneration of complicated skin tissues and epidermis layers.[1] Because keratinocytes can proliferate, migrate, and produce essential extracellular matrix components, they play a vital role in skin regeneration and wound healing.[2] The use of stem-cell-based approaches has gained significant attention in cases where the natural supply of keratinocytes is inadequate or impaired.

Meanwhile, stem cells, particularly adipose-derived stem cells (ADSCs), have shown great promise in tissue engineering and regenerative medicine due to their unique properties.[3−10] Since ADSCs are easy to access, are abundant, and have

multilineage plasticity, they have emerged as a promising skin regeneration candidate.[11] They secrete various growth factors that promote wound healing, making them ideal for enhancing tissue renewal.[12,13] Although ADSCs have the potential to differentiate into functional keratinocytes, their efficient and controlled differentiation remains a challenge.[14]

Some growth factors, such as epithelial growth factor (EGF),[15] keratinocyte growth factor (KGF),[16] fibroblast growth factor (FGF),[17] and hepatocyte growth factor (HGF),[18] have been used either individually or in combination with other inducers to promote the differentiation of ADSCs

into keratinocyte-like cells. Despite playing a pivotal role in promoting cell proliferation, angiogenesis,[19] and collagen synthesis—essential for efficient tissue repair—platelet-derived growth factor (PDGF-BB) has not yet been utilized to differentiate ADSCs into keratinocyte-like cells. Additionally, in patients with slow-healing wounds, this compound's secretion is less than the required level; therefore, its administration helps speed up the healing of these patients' wounds.[20] However, topical delivery of PDGF is severely limited due to its short half-life and potential to exert unwanted effects.[21] To overcome the limitations of conventional differentiation protocols, incorporating PDGF-containing bioactive nanospheres within gelatin—collagen (GC) hydrogel scaffolds presents a promising solution. The biocompatible copolymer of polycaprolactone and polyethylene glycol (PCL—PEG-PCL) has been used frequently for encapsulation.[22−29] PCL—PEG-PCL is able to encapsulate proteins due to being amphiphilic. The hydrophilic polyethylene glycol block is close to the encapsulated protein molecule polycaprolactone blocks arranged outward. Sustaining of protein release from PCL—PEG-PCL has been described in a few investigations,[30−32] but it has never been utilized to encapsulate PDGF-BB, according to the bibliography. Nowadays, various experimental design methods are used to develop new drug formulations and make optimal use of materials and preparation methods, such as the response surface methodology.[33−37] These designs help researchers determine the simultaneous effect of different factors on the efficiency and achieve the best formulation. Therefore, we used the Box—Behnken method to design and optimize experiments involving the preparation of PDGF-loaded PCEC nanospheres.

Nanospheres allow precise control over growth factor release kinetics, ensuring sustained and local delivery to ADSCs within the scaffold microenvironment. ADSC differentiation can be enhanced through this approach, and keratinocyte-like characteristics can be encouraged, simulating natural paracrine signaling in skin regeneration. An important challenge in this study is developing a reliable method for incorporating PDGF-containing bioactive nanospheres into a suitable hydrogel scaffold in order to control the growth factor release kinetics.

The choice of scaffold material and structure significantly influences cell behavior and tissue regeneration outcomes. Several studies have demonstrated that GC hydrogelic scaffolds exhibit favorable biocompatibility and mechanical properties, allowing cells to attach, proliferate, and deposit extracellular matrix.[38−40] For PDGF-containing bioactive nanospheres to be successfully incorporated into the scaffold matrix, the interaction among the nanospheres, GC hydrogel, and cells must be carefully considered. Achieving regenerative outcomes requires an optimized scaffold design with uniform nanosphere distribution, adequate stability, and sustained release of growth factor.

Given that, we investigated the potential of PDGF-BB and a GC porous scaffold to enhance the differentiation of human ADSCs to keratinocyte-like cells. We first designed and optimized the preparation of PDGF-loaded PCEC nanospheres by using the Box—Behnken method. We then encapsulated PDGF-BB in PCEC nanospheres embedded in a 3D extracellular matrix-like sponge. Subsequently, we assessed the release of PDGF-BB from nanospheres and scaffolds and its bioactivity after release. Finally, we examined the effects of integrated scaffolds on the in vitro keratinocyte-like cell differentiation of hADSCs by using Western blotting,

RT-PCR analysis, and microscopic observation. The achievement of these objectives may help to develop wound healing strategies, leading to improved therapeutic outcomes and quality of life for patients with chronic wounds and extensive skin injuries.

2. MATERIAL AND METHODS

2.1. Materials and Reagents. Human recombinant platelet-derived growth factor-BB (PDGF-BB,99.9%) was purchased from PeproTech, and the PDGF ELISA kit was purchased from Abcam (Canada). Bovine collagen (acid-soluble collagen; Type I) was received as a friendly gift from the laboratory of Dr. Khosh Fetrat. Gelatin (porcine skin, type A), poly(vinyl alcohol) (M 85k), and stannous 2-ethyl hexanoate (stannous octoate, $Sn(Oct)_2$) were purchased from Sigma-Aldrich (USA). Polycaprolactone (PCL, Mn: 45000), ε-caprolactone, polyethylene glycol (PEG, Mn: 4000), acetic acid (glacial), and tetrazolium salt 3-(4, 5-dimethylthiazol-2-yl)-2,5-diphenyltetrazolium bromide (MTT) were obtained from Sigma-Aldrich (USA). Glutaraldehyde (25% aqueous solution) and all solvents were purchased from Merck Inc. Dulbecco's modified Eagle's medium (DMEM-high glucose), Ham's F-12 medium, and penicillin—streptomycin were also obtained from Gibco (USA). Fetal bovine serum (FBS) was purchased from PAN-Biotech (Germany).

2.2. Development of PD@PCEC Nanospheres. The PCEC copolymer was synthesized through ε-CL ring opening according to a previous protocol[32] (please refer to Figure 1 for a visual representation of the process). Nanospheres containing PDGF-BB were prepared using a double-emulsion process (w/o/w). The procedure begins with the preparation of a 1 mL aqueous solution of PDGF-BB at a known concentration of 300 ng/mL. This solution is dropwise
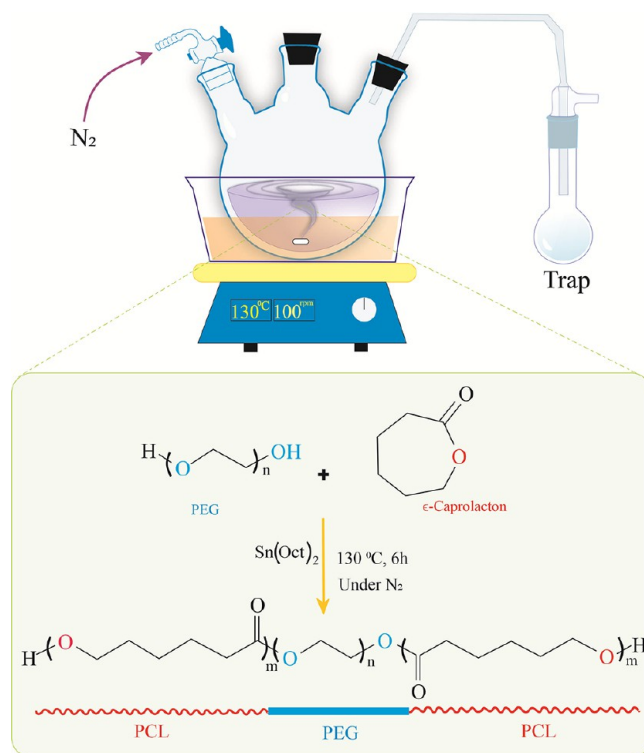
Figure 1. Overview of the synthesis steps for the PCEC triblock copolymer using ε-CL ring opening.

injected into the PCEC copolymer solution in 2 mL of methylene chloride (100 mg/mL) via a syringe (G = 22), followed by application of ultrasound to form a w/o emulsion. The resulting solution is emulsified by combining it with a solution of PVA in deionized water (PVA concentration: 0.56%). The emulsion is stirred at room temperature for 30 min at 200 rpm. Deionized water (50 mL) is added to the emulsion, and the mixture was stirred for another 30 min. The stirring continued until the methylene chloride solvent is completely evaporated, which is equivalent to 139 min. The PD@PCEC nanospheres were collected by centrifugation, washed twice with distilled water, lyophilized, and stored at −20 °C until use. The optimal parameters for preparing PD@PCEC nanospheres were obtained by designing the experiment by using the Box−Behnken method.

2.3. Obtaining the Factors Affecting the Encapsulation Efficiency and Their Optimal Values with the Response Surface Design Method.

Previously, the OFAT method was used to prepare and optimize new drug delivery systems. This means that in each experiment, instead of examining the simultaneous effect of different factors on efficiency, they examined only the effect of one factor. This method required many experiments, and it was usually impossible to achieve optimal conditions. Nowadays, to save time and money, various experimental design methods are used to develop new drug formulations and optimize materials and preparation methods, such as the response surface methodology.[41−43]

In this project, using the designed experiments, a two-level Box−Behnken method was used to evaluate the effect of the stirring rate, stirring duration, PVA concentration, and PDGF-BB concentration (Table 1) on the encapsulation efficiency

(EE). Minitab statistical software 20.4.0.0 was applied to examine the data, optimize the experimental settings, and examine each parameter at two alternative levels (−1 and +1). The minimum and maximum values for parameters were adjusted on the basis of the laboratory-based preliminary study results.

Twenty-seven batches of experiments were designed (Table 2), and the EE of produced particles was evaluated by dividing the mass of PDGF-BB loaded into the PCEC nanospheres by the overall mass of PDGF-BB.

2.4. Fabrication of Cross-Linked Gelatin−Collagen Hydrogel Scaffolds.

A 9% by weight solution of porcine gelatin type A in deionized water was prepared with the help of heat and mixed with an equal volume of bovine collagen type 1 solution (1 wt %) in 1% acetic acid for 4 h at 40 °C.

Then, PD@PCEC nanospheres (concentration of 10 ng/mL of PDGF), and unloaded nanospheres, were added to the gel/col solution in two separate groups and stirred for 5 min.

After the glutaraldehyde solution (2.5%, v/v) was dropped into the mixtures and stirred for 5 min at 35 °C, the resulting mixture was poured into plastic molds of appropriate size and the hydrogel was hardened at room temperature.

The scaffolds were frozen at −20 °C and lyophilized using a freeze-dryer at −70 °C for 48 h. To prevent cytotoxicity, the remaining aldehyde groups in the scaffolds, after cross-linking with glutaraldehyde, were blocked by immersing the lyophilized scaffolds in a 50 mM glycine solution for 2 h.

Finally, the scaffolds were removed from the glycine solution, washed twice with deionized water, and lyophilized in a freeze-dryer at a temperature of −70 °C.

2.5. Characterization of PD@PCEC Nanospheres and Prepared Scaffolds.

2.5.1. FTIR Analysis. A Bruker (Germany) FTIR spectrometer was used to record the I.R. spectrum of the PCEC copolymer, primary monomers, gelatin, collagen, and prepared scaffolds.

2.5.2. ^{1}HNMR. Nuclear magnetic resonance spectra were recorded using a Bruker AC 80 spectrometer operating at a frequency of 400 MHz and CDCl$_3$ as the solvent. The copolymer structure was characterized by the peaks observed in the ^{1}HNMR spectrum.

2.5.3. XRD Analysis. A Bruker D8 ADVANCE diffractometer (Germany) with operating conditions set at 40 kV and 30 mA and a 2θ angle range from 5 to 70° was used to record the XRD patterns of copolymers and monomers.

Table 1. Experimental Conditions of Box−Behnken Design for Preparation of PDGF-BB-Loaded Nanospheres by a Double-Emulsion Process (w/o/w)

			levels	
			min	max
factors		coded units	−1	+1
#1	stirring rate (rpm)	X1	200	900
#2	stirring duration (min)	X2	30	150
#3	PVA concentration (%)	X3	0.4	1.0
#4	PDGF-BB concentration (ng/mL)	X4	200	300

Table 2. Design of the Experiments and the Obtained Results

trial no.	X1 rpm	X2 min	X3%	X4 ng/mL	EE (mean ± SD) %	trial no.	X1 rpm	X2 min	X3%	X4 ng/mL	EE (mean ± SD) %
1	550	90	1.0	200	56.2 ± 0.25	15	900	90	0.7	300	72.6 ± 0.04
2	200	90	0.7	200	62.9 ± 0.18	16	550	90	0.7	250	69.5 ± 0.05
3	200	30	0.7	250	68.0 ± 0.50	17	550	30	1.0	250	66.6 ± 0.14
4	200	150	0.7	250	81.0 ± 0.35	18	200	90	1.0	250	77.6 ± 0.25
5	550	90	0.4	300	78.2 ± 0.42	19	900	30	0.7	250	65.4 ± 0.13
6	200	90	0.7	300	84.5 ± 0.44	20	550	150	1.0	250	66.9 ± 0.48
7	900	90	0.7	200	50.6 ± 0.10	21	550	150	0.7	200	54.7 ± 0.10
8	900	150	0.7	250	58.4 ± 0.25	22	900	90	0.4	250	61.7 ± 0.14
9	550	30	0.7	200	47.0 ± 0.18	23	550	150	0.4	250	66.5 ± 0.12
10	550	90	0.4	200	53.0 ± 0.19	24	550	90	1.0	300	76.8 ± 0.37
11	900	90	1.0	250	66.1 ± 0.005	25	200	90	0.4	250	74.5 ± 0.18
12	550	90	0.7	250	71.0 ± 0.17	26	550	150	0.7	300	76.5 ± 0.30
13	550	30	0.7	300	74.2 ± 0.18	27	550	30	0.4	250	62.1 ± 0.23
14	550	90	0.7	250	70.9 ± 0.19						

2.5.4. Particle Size Distribution and Zeta Potential Measurement. Determination of the zeta potential (ζ) was performed using a Nanotrac wave (Microtrac Inc., USA) Zetasizer at 26 °C. To determine the zeta potential of the PD@PCEC nanospheres, they were dispersed in deionized water to ensure no diffusion and Brownian motion. The particle size distribution was determined by the DLS method.

2.5.5. Encapsulation Efficiency (% EE). After rinsing PDGF-loaded nanospheres with deionized water two times, the resulting solution was added to the centrifuged nanosphere supernatant. Then, the growth factor concentration in this solution was determined using an ELISA kit. The amount of PDGF-BB loaded into the nanospheres was calculated by subtracting the amount of unloaded PDGF-BB from the total protein initially added to the solution. Finally, the % EE was subsequently calculated by eq 1. The average of two experiment replications and standard deviation was reported (Table 2).

$$\%EE = \frac{\text{total PDGF} - \text{unloaded PDGF}}{\text{total PDGF}} \times 100 \qquad (1)$$

2.5.6. Morphology of Nanospheres and Scaffolds. The structure of the PD@PCEC nanospheres was examined by TEM (Philips EM208S) imaging at 200 kV. A droplet of the nanosphere solution (10 μL) was placed onto the copper micro grid for TEM analysis. After the solution dried, data were collected by using an applied accelerating voltage. To investigate the morphology of scaffolds, a MIRA3 FEG-SEM, TESCAN (Czech) scanning electron microscope (SEM) was applied.

2.5.7. Mechanical Strength of Scaffolds. A Zwick tensile testing machine (Z010, Zwick/Roell, and Ulm, Germany) was used to determine the mechanical strength of the scaffolds (dimensions = $10 \times 10 \times 0.2$ cm^3) at a constant tensile deformation rate of 2 mm/min in the dry state at 25 °C. The stress−strain curve of the samples was drawn, and the corresponding Young's modulus of each scaffold was calculated.

2.5.8. Porosity of Scaffolds. Methods such as BET (adsorption and desorption of gaseous nitrogen) or liquid replacement methods can be used to determine the porosity of scaffolds. Because of the prepared scaffolds' high porosity and low density, it was difficult to stabilize them inside the gas porosimeter (BET) cells during the degassing stage. Therefore, it was preferable to use the second method (liquid replacement method) to solve this problem. To determine the porosity of the scaffolds, equal-sized pieces of the scaffolds were immersed in a graduated cylinder containing a specific volume of absolute ethanol (V_1, cm^3) for 10 min. Scaffolds were removed from the graduated cylinder, and the volume of the remaining alcohol was recorded (V_3). V_2 was considered the volume of the scaffolds and was calculated from their dimensions. The volume of absorbed alcohol in the scaffold was obtained by subtracting V_3 from the volume of V_1. The percentage of scaffold porosity was obtained from eq 2.

$$\%\text{porosity} = \frac{\text{volume of absorbed ethanol}}{\text{volume of scaffold}} \times 100 \qquad (2)$$

2.5.9. Swelling Behavior. The experiments related to the swelling of the scaffolds were performed by immersing the weighted pieces of the scaffolds with specific dimensions in PBS solution with pH 7.4 for 120 h and 37 °C.[44] At specific time intervals, the scaffolds were removed from the PBS

solution, and after drying their surface, their weight was measured and recorded with an analytical balance. The swelling ratio of the scaffolds was then obtained from the following equation.[45,46]

$$\text{swelling ratio} = \frac{W_2 - W_1}{W_1} \qquad (3)$$

where W_1 and W_2 are the initial weight of the scaffolds and the weight of the scaffolds after swelling, respectively.

2.5.10. Degradation Profile of Scaffolds. The degradation profile of the fabricated scaffolds for tissue engineering is particularly important. In this study, the degradation of 3D scaffolds was investigated in a PBS solution and a solution containing a specific concentration of lysozyme according to the ASTM method (F-1635-95). The dried and precisely weighed scaffold samples (w_1) were submerged in PBS solution with pH 7.4 and a PBS solution containing 13 mg/L of lysozyme enzyme. The samples were then incubated at 37 °C for a specified time. The concentration of lysozyme was chosen to be equivalent to its concentration in human blood.[47] At specific time intervals (7, 14, and 21 days for degradation in PBS solution and 1, 2, 4, 6, and 8 h for degradation in PBS solution containing lysozyme), the samples were removed from the degradation environment and weighed after 24 h of exposure to air (w_2). The percentage of degradation of scaffolds at any specified time was calculated using eq 4.[48]

$$\text{degradation\%} = \frac{W_1 - W_2}{W_1} \times 100 \qquad (4)$$

Each experiment was performed three times, and the results were reported as the average of the results of the three experiments and standard deviation.

2.6. In Vitro Release of PDGF-BB from Nanospheres and Scaffolds. The following method was used in vitro to investigate PDGF-BB release from PD@PCEC nanospheres and PD@PCEC@GC scaffolds for 504 h.[49] Encapsulated PD@PCEC nanospheres (10 mg) were dispersed in 1 mL of phosphate buffer (pH 7.4) and incubated at 37 °C with continuous shaking. The supernatant of samples was removed at specified intervals, including 8, 120, 240, 360, and 504 h, and transferred to clean microtubes to be stored at −21 °C until ELISA analysis. Then, 1 mL of fresh phosphate buffer solution (pH 7.4) was added to the remaining nanospheres in each microtube and the microtubes were transferred to the shaker incubator. The amount of PDGF-BB released in the samples was determined using a sandwich ELISA kit and the manufacturer's method. These steps were repeated using weighed PD@PCEC@GC scaffold pieces to determine the amount of PDGF released. Each experiment was conducted twice.

2.7. Bioactivity Assay of the Released PDGF-BB. The bioactivity of the released PDGF-BB was assessed based on its influence on human gingival fibroblast cells (HGFCs), whose cell division rate depends on the biologically active dosage of the growth factor.[50] HGFCs were seeded in a 24-well plate at a density of 1000 cells per well. They were allowed to adhere overnight and then subjected to nutrient deprivation for 2 days by replacing the medium with DMEM containing 0.5% FBS. After a 2-day period, the medium was replaced with a complete medium consisting of 10% FBS and 1% penicillin−streptomycin (PS). The concentration of released PDGF-BB in the supernatant was quantified using ELISA at time intervals

of 8, 120, 240, 360, and 504 h. The resulting concentrations were subsequently diluted to 10 ng/mL in a complete medium. The impact of these supernatant samples on HGFCs was assessed by comparing them to cells cultured with 10 ng/mL of fresh PDGF-BB as a positive control and with full media (without the growth factor) as a negative control. The cells were incubated for a duration of 3 days, and the cell growth rate was evaluated using the MTT assay, in accordance with ISO10993-5.

2.8. Cell Culture. *2.8.1. Sterilization of the Scaffolds, Cell Seeding, and Differentiation Study of hADSCs to Keratinocyte.* The second passage of hADSCs purchased from the Skin Research Center of the University of Tehran, Iran, was used in this part of the study. Cells were incubated in DMEM-high glucose (Gibco, Cat. No. 11965092) supplemented with 10% FBS (PAN-Biotech, Cat. No. P30-1302) at 37 °C for 48 h in 95% oxygen and 5% carbon dioxide. The culture flask was washed with PBS after 48 h to remove nonadherent cells. The medium was changed every 48−72 h until 80−90% confluence was reached with fibroblast-like adherent cells. hADSCs were harvested using trypsin/EDTA 0.25% (Gibco, Cat. No. 25200056) and passaged for further passages. The third passage of cells was applied.[51] The synthesized cylindrical scaffolds were mounted with an insert in the wells of a 24-well cell culture plate. Then, a 70% ethanol solution was poured onto the scaffolds inside each well. After the ethanol was drained for 2 h, the scaffolds were washed twice with PBS. Then, DMEM culture medium was poured onto the scaffolds overnight in an incubator. The culture medium was emptied from the wells the next day, and 10^5 cells were cultured in each well. A 70:30 DMEM/F12 culture medium was used for the culture plus 10% FBS. The culture medium was changed every 2 days, and on the third day of culture, an all-trans retinoic acid (ATRA) solution (10 ng/mL) was added to half of the wells. On the 4th, 10th, and 21st days, the morphology of the cells was examined under a microscope. On the 21st day, when the cells exhibited a change in morphology, becoming spherical or tetrahedral, RNA was extracted from the cells. Subsequently, RT-PCR was performed to confirm the differentiation. Western blot analysis was performed on another part of each group's cells to confirm the differentiation.

2.8.2. Scaffold Preparation for the Adhesion Test. After 5 h of cell culture on the scaffold, the culture medium was discarded; the scaffold was washed twice with PBS and fixed with 2.5% glutaraldehyde for 2 h. Then, glutaraldehyde was drained, and after washing the scaffold with PBS, we added 1% osmium tetroxide solution and allowed the scaffold to remain in the incubator for 1.5 h.[52] We drained the solution and placed the samples in a desiccator overnight and sent them for SEM imaging the next day.

2.8.3. Microscopic Observation Using a Light Microscope. The seeded hADSCs on scaffolds were trypsinized at different intervals (3, 10, and 21 days) and resuspended in freshly prepared flasks at those intervals. Using a light microscope (Motic, Hong Kong), changes in cell morphology were observed 1 day after cells were attached to flasks.

2.8.4. Biocompatibility Study. The MTT assay was used to quantify the viability and proliferation rate of hADSCs in 3D nanocomposite hydrogels for 14 days. The proliferation of hADSCs was examined after 1, 3, 5, 7, and 14 days of culture on the PD@PCEC@GC scaffold, GC scaffold, and PDGF-BB-containing flasks. ADSCs cultured in a flask in DMEM/F-12 medium were considered the control group. After sterilization

and preparation, the scaffolds were placed in a 96-well cell culture plate and 50,000 cells were cultured in each well. To assess cellular viability, MTT tests were conducted according to ISO10993-5. 500 μL of MTT solution (2.0 mg/mL) was added to each culture well. The MTT reaction medium was removed after 3 h, and 2.0 mL of dimethyl sulfoxide was added. Optical densities (ODs) were determined by using a spectrophotometer at 570 nm.

2.8.5. Western Blotting. Western blotting was performed using previous protocols.[53,54] Using RIPA buffer, cells were lysed. Centrifugation at 14,000 rpm for 20 min at 4 °C was used to remove the debris. A Bradford Protein Quantification kit (DB0017, DNAbiotech, Iran) was used to determine the protein concentration. An equal volume of a Laemmli sample buffer was mixed with the cell lysates. After boiling for 5 min, the lysates were subjected to SDS-PAGE and subsequently transferred to an Immun-Blot polyvinylidene difluoride membrane (Cat No. 162-017777; Bio-Rad Laboratories, California, USA). The membranes were blocked with 5% BSA in 0.1% Tween 20 (Sigma-Aldrich, Missouri, USA) for 1 h. The membranes were incubated for 1 h at room temperature with anticytokeratin 19 (Cat No. ab52625, Abcam), anti-cytokeratin 18 (Cat No. ab133263, Abcam), anti-involucrin (Cat No. ab181980, Abcam), and anti-GAPDH-loading control antibodies (Cat No. ab9485, Abcam). The membranes were then washed three times with TBST and incubated with goat antirabbit IgG H&L (HRP) (Cat No. ab6721; Abcam). The membranes were incubated with enhanced chemiluminescence (ECL) for 1−2 min. Protein expression was normalized to glyceraldehyde-3-phosphate-dehdrogenase (GAPDH). The gel analyzer version 2010a software (NIH, USA) was used to calculate the density of protein bands by dividing each band's area under the curve by its GAPDH band's area under the curve and comparing the calculated values between groups.[55]

2.8.6. RT-PCR Analysis. A quantitative real-time polymerase chain reaction (RT-PCR) test was performed to evaluate the expression of keratinocyte-specific genes, such as cytokeratin 18 (CK-18), cytokeratin 19 (CK-19), and involucrin, after 21 days of cell culture on the scaffolds. The primer sequences designed to perform the test are listed in Table 3. Total RNA

Table 3. Sequences of Primers Used for RT-PCR

gene name	direction	primer sequence (5′−3′)
GAPDH	forward	ACCCACTCCTCCACCTTTGA
	reverse	ACGAATTTGGCTACAGCAACAG
K18	forward	GGCGAGGACTTTAATCTTGGT
	reverse	ACCACTTTGCCATCCACTATC
K19	forward	CCATGAGGAGGAAATCAGTACG
	reverse	CTTCGCATGTCACTCAGGAT
involucrin	forward	GCCTTACTGTGAGTCTGGTTG
	reverse	TCATTTGCTCCTGATGGGTATT

was extracted manually from cells placed on the scaffolds, according to the manufacturer's protocol.[56] Briefly, they were washed with a cold PBS solution after the scaffolds were homogenized with a homogenizer. Next, 1 mL of TRIzol (Invitrogen, USA) was poured into each homogenized scaffold. After 2 min, the TRIzol/cell solution was transferred to a 1.5 mL Eppendorf tube using a pipet. After keeping at room temperature for 5 min, 250 μL of chloroform was added to each tube and vigorously shaken for 15 s.

After 5 min of storage at room temperature, the contents of the tubes were centrifuged for 5 min at 10,000 rpm. After the tubes were removed from the centrifuge, the upper transparent layer was removed using a pipet. This layer was poured into clean 1.5 mL Eppendorf tubes, and 550 μL of 2-propanol was added to each tube. The tubes were maintained at room temperature for 5 min and then centrifuged for 25 min at 14,000 rpm. The samples were placed on ice. After draining the isopropanol with a pipet, 1 mL of 70% ethanol was dissolved in DEPC. This solution was added to the white sediment at the bottom of the tubes. After the contents of the tubes were gently mixed, the tubes were centrifuged at 9500 rpm. After the ethanol was poured out of the tubes, the pellet remaining at the bottom was air-dried and then dissolved in 20 μL of DEPC. From these obtained stock solutions, diluted solutions with a ratio of 1:40 were prepared and the absorption rate at 260 nm and the absorption ratio at 280/260 were obtained using nanodrop (nanodrop; Thermo, Wilmington, USA). The ratios obtained in all samples were higher than 1.8.

Subsequently, RNA was reverse transcribed into cDNA using the cDNA synthesis kit (BioFact 2 Step 2X RT-PCR Premix, South Korea). cDNAs were amplified using a SYBR Green Real-Time PCR Master Mix (BioFact 2 Step 2X RT-PCR Master Mix, South Korea). The relative expression is the ratio of the specific gene's expression to that of GAPDH, a housekeeping gene.

2.9. Statistical Analysis. All results are reported as the mean standard deviation (SD) from at least three studies. Statistical analyses were performed using GraphPad Prism (version 9). The differences between the two groups were analyzed using the paired multiple t tests. A one-way variance analysis was employed to examine differences between three or more groups. Differences were deemed statistically significant when $p < 0.05$ (*), $p < 0.01$ (**), $p < 0.001$ (***), and $p < 0.0001$ (****), whereas ns indicates that the difference was not statistically significant.

3. RESULTS

3.1. Preparation and Optimization by Experimental Design. *3.1.1. Preparation.* Figure 2 shows a schematic representation of growth factor-loaded polymer nanoparticles' production. In the first step, the organic phase is emulsified by
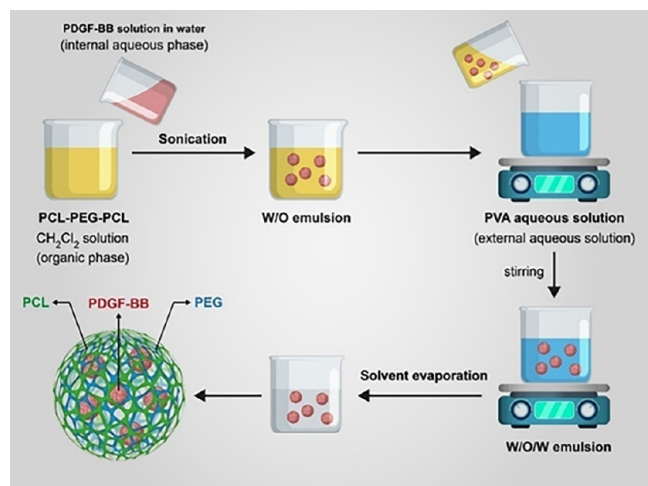
Figure 2. Schematic representation of the preparation of PD@PCEC nanospheres.

the oil-in-water (o/w) process in the aqueous phase. In the second step, evaporation of CH_2Cl_2 from the emulsion droplets causes the copolymer to condense. Finally, increasing the polymer concentration above the critical level causes the deposition of nanoparticles in the organic phase.

3.1.2. The Effect of the Experimental Variables on the EE. The results in Table 2 show the mean value of EE obtained from the two studies and its standard deviation for each combination of the four specified parameters. Additionally, the graphs in Figure 3A illustrate the evolution of the mean value of the EE concerning these components from minimum to maximum values.

Graph X1 versus EE shows that as the solution's stirring rate increased, the nanoparticles formed became smaller because fewer copolymer molecules were placed next to each other and formed due to the increasing irregularity of nanoparticles. Therefore, to increase the encapsulation efficiency, the stirring rate must be reduced. The decrease in EE is not entirely uniform with an increasing stirring speed. After reaching a speed of 550 rpm, the encapsulation should be reduced with a gentler slope.

Graph X2 versus EE shows that as the stirring duration increases from 30 to 90 min, the EE increases sharply but remains almost constant from 90 to 150 min. This may be because more time is spent disrupting the formed nano-particles. Due to the low zeta potential (5.2 mV), many nanoparticles are clumped together and the aggregation phenomenon occurs. Determining the particle size of nano-particles with a size meter confirms this (Figure 7b). On the other hand, considering that the EE remains constant from 90 min onward, it can be concluded that the adhesion of the nanoparticles is completed in 90 min. Then, no more aggregation occurs, so the particles do not become larger and the EE does not increase.

Graph X3 shows that increasing the concentration of PVA did not significantly affect encapsulation. Contrary to what can be seen in some previous literature, increasing the PVA concentration is only slightly effective in increasing the particle size of the nanoparticles.[57] This contrasting effect is negligible. Graph X4 versus EE shows a significant increase in encapsulation with increasing PDGF concentration. On the other hand, increasing the PDGF concentration also increases the nanoparticle's particle size. This observation can be attributed to larger nanoparticles forming when more encapsulated material is available to the copolymer molecules, increasing the encapsulation percentage, as seen in the previous paragraphs. After the PDGF concentration reaches 250 ng/mL, the increase in encapsulation increases slightly. The analysis of variance (ANOVA) shows that the interaction between some of the factors affects the EE (Figure 3B). This figure shows that there is a significant interaction between factors X1 and X2 ($P < 0.05$), which also increases with the increasing X1. There is a significant interaction between X2 and X4 ($P < 0.05$), but between X1 and X3 ($P > 0.05$), between X1 and X4 ($P > 0.005$), between X2 and X3 ($P > 0.05$), and between X3 and X4 ($P > 0.05$), no interaction was observed.

3.1.3. Use of the Box−Behnken Experimental Design. The current research focuses on the four criteria listed in Table 1, each with two values. With 27 experiments, this experimental program analyzes the effect of a relevant selection of experimental parameters on a process's performance (EE). To simplify the modeling approach, the influence of each
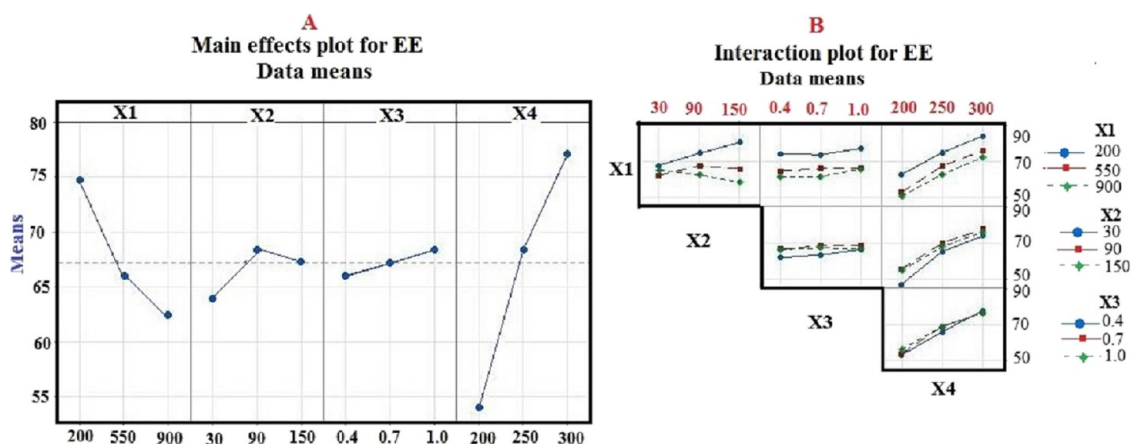
Figure 3. (A) Effects of the variables under investigation (X1, X2, X3, and X4) on the mean value of the EE. (B) Interaction plots of experimental variables and their effects on the EE. The blue lines correspond to the lower level of the factors, the red lines correspond to their middle level, and the green lines correspond to their high level.
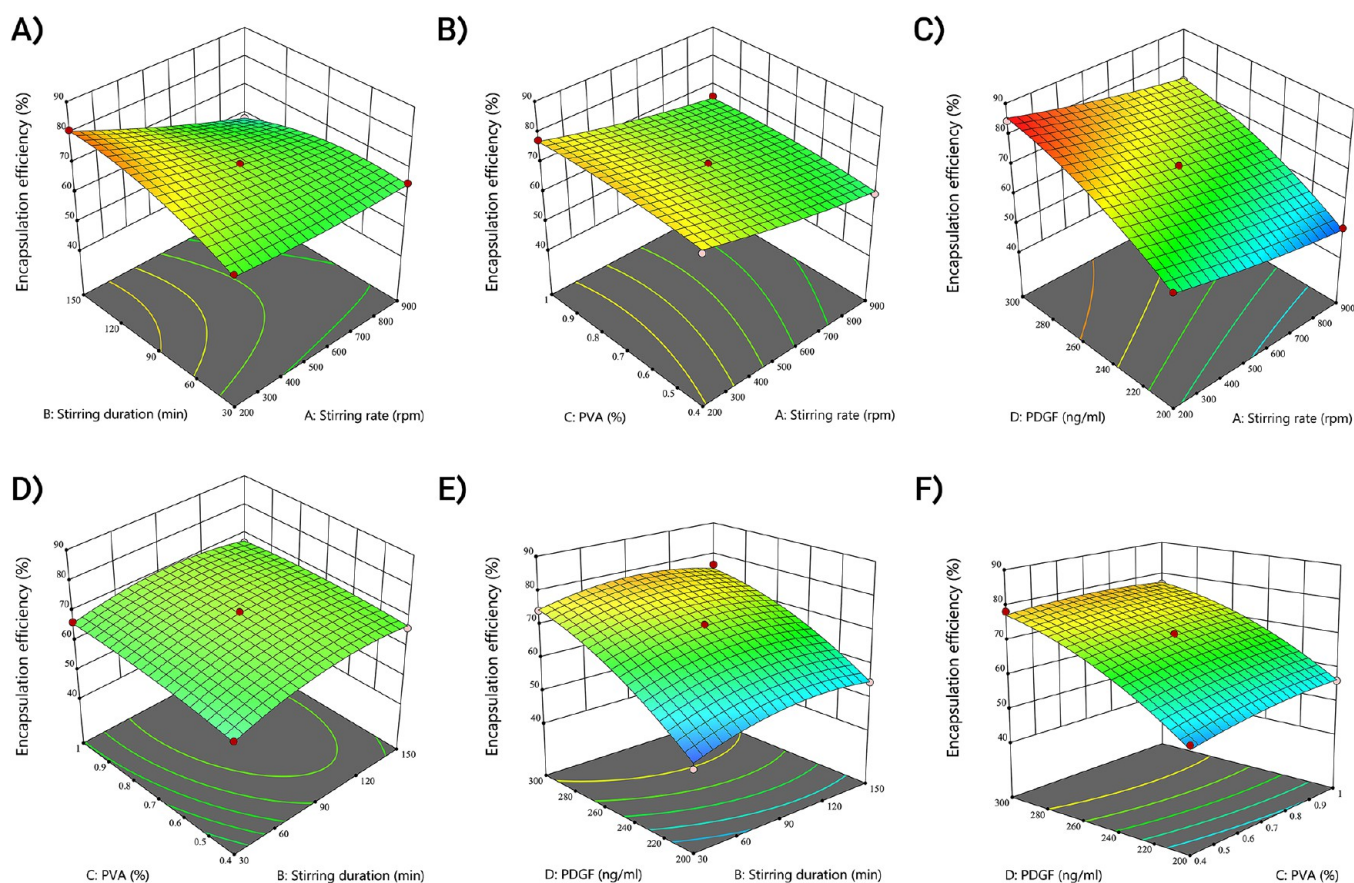
Figure 4. Response surface for EE with respect to (A) X1, X2; (B) X1, X3; (C) X1, X4; (D) X2, X3; (E) X2, X4; and (F) X3, X4.

element was represented by a linear variation. The correlation between the resulting response (EE) and the four specified factors (X1, X2, X3, X4) can be represented by the following polynomial model when the findings are statistically analyzed (eq 5):

$$
\begin{aligned}
EE\% = {}& -127.7 - 0.0081 X1 + 0.4906 X2 + 45.3 X3 \\
& + 1.038 X4 + 0.000008 X1 \times X1 - 0.000992 X2 \\
& \times X2 - 13.43 X3 \times X3 - 0.001433 X4 \times X4 \\
& - 0.000238 X1 \times X2 + 0.00310 X1 \times X3 \\
& + 0.000006 X1 \times X4 - 0.0569 X2 \times X3 \\
& - 0.000450 X2 \times X4 - 0.0767 X3 \times X4
\end{aligned}
\tag{5}
$$

On the six three-dimensional (3D) plots given in Figure 4, the impacts of the independent factors and their interactions

on EE may be visualized. The observed surfaces were created by graphing EE's reaction against X_i and X_j's independent variables while maintaining the other two variables at their median values.

Each three-dimensional plot illustrates the possible combinations of the two test variables and represents the regression equation in graphical form. This plotting technique is advantageous for determining the link between independent and dependent variables.

A variance test was performed to establish the significance of the polynomial mathematical model. Table 4 summarizes the results of the second-order model fitting. This analysis established the model's significance by examining the F and p values.[58]

Table 4. Analysis of Variance (ANOVA) for the Model[a]

source	DF	SS	MS	F-value	p-value probability > F
model	14	2368.25	169.16	136.89	<0.0001
error	12	14.83	1.24		
total	26	2383.08			

[a]DF: degree of freedom; S.S.: sum of squares; MS: mean squares.

3.1.4. Optimal Parameters for the Formulation of PCEC Nanoparticles Loaded with PDGF-BB. The above model is primarily concerned with determining the elements that influence the EE of PDGF-BB-loaded nanoparticles. The results of the statistical technique are in the following desirable optimum factors: X1 = 200 rpm, X2 = 139.1 min, X3 = 0.56%, and X4 = 300 ng/mL. The model predicts an EE of 87.7% under these optimum conditions. An optimal experiment value was compared to the mathematically anticipated one to

validate this model. This validation established the model's correctness, as the mean value of EE calculated from the experiments was 85.4%. Thus, using a paired t test, the divergence between theoretical and experimental values of EE can be judged nonsignificant at $p > 0.05$, indicating that predicted optimization occurs in practice.

3.2. Characterization of Nanospheres and Scaffolds. The FTIR spectra of the PCEC without PDGF, PD@PCEC, PDGF-BB, and scaffolds without and with encapsulated PDGF-BB are shown in Figures 5a and 6. The intense bands at 1726 and 1109 cm^{-1} from the FTIR spectrum of PCEC are related to the stretches of carboxylic ester (C=O) and ether (C−O) groups, indicating the successful formation of the PCL−PEG-PCL copolymer. The absorption peak at 3441 cm^{-1} belongs to the free OH group of the PCL units. The bands at 2943 and 2863 cm^{-1} are due to the C−H stretch.[59,60]

On the other hand, the band that appeared at 1558 cm^{-1} in the FTIR spectrum of PD@PCEC nanospheres can be attributed to the stretch of the N−H primary and secondary amides.[61] This peak is not observed in the FTIR spectrum of PCEC without a growth factor. Therefore, we can confirm the successful encapsulation of growth factors in polymer nanospheres. In addition, by comparing the FTIR spectra of GC and PD@PCEC@GC, the presence of a peak related to the N−H stretching of the first and second type amide groups of PDGF at 1558 cm^{-1} was observed in the spectrum of the second scaffold. The presence of a growth factor inside this scaffold was confirmed.

Figure 5b shows the copolymer's ^{1}HNMR spectra. The 4.05, 2.3, 1.65, and 1.37 ppm peaks correspond to the oxycarboxy-1,5-pentamethylene units in polycaprolactone. The peak of the methylene protons of oxyethylene units belonging to PEG appears at approximately 3.63 ppm.[62]
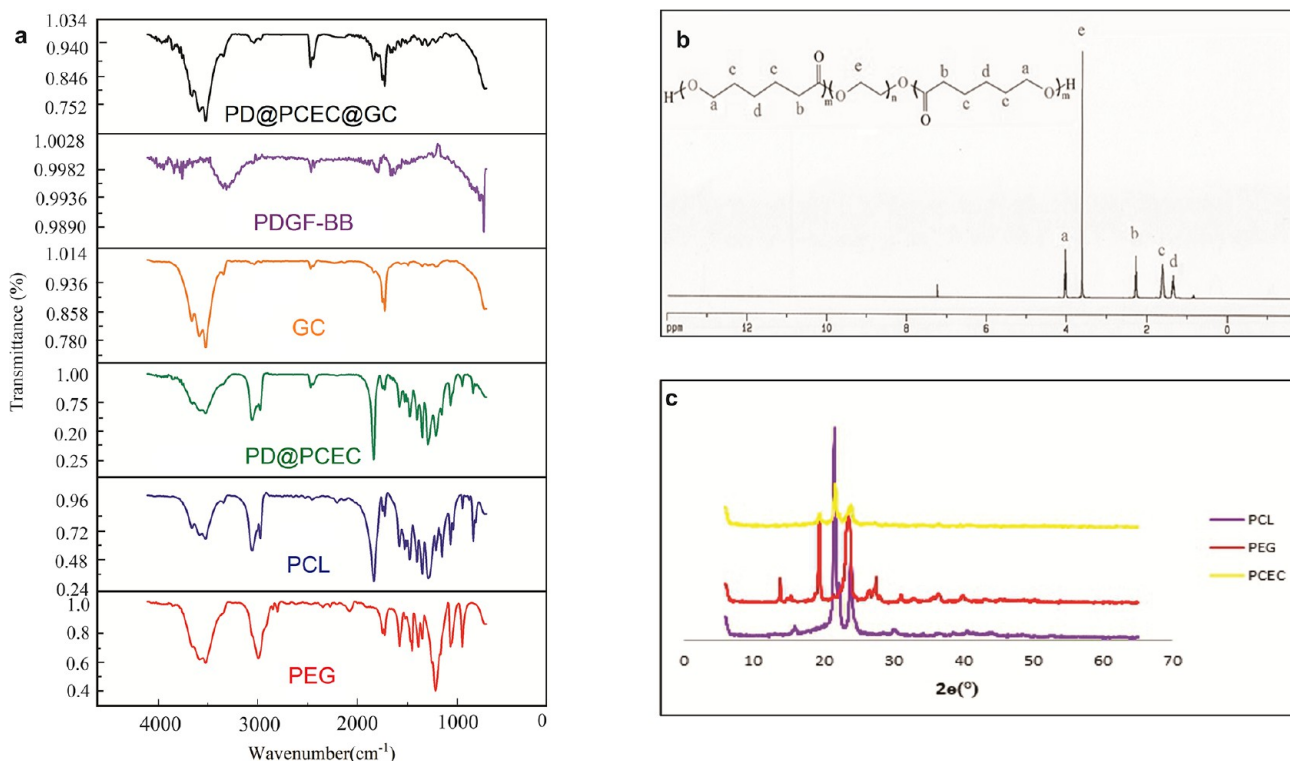
Figure 5. Characterization of PCEC nanospheres. (a) FTIR spectra of PD@PCEC@GC, PDGF-BB, GC, PD@PCEC nanospheres, PCL, and PEG4000. (b) ^{1}HNMR spectrum of the PCEC triblock copolymer in CDCl$_3$. (c) XRD patterns of PCL, PEG 4000, and PCEC.
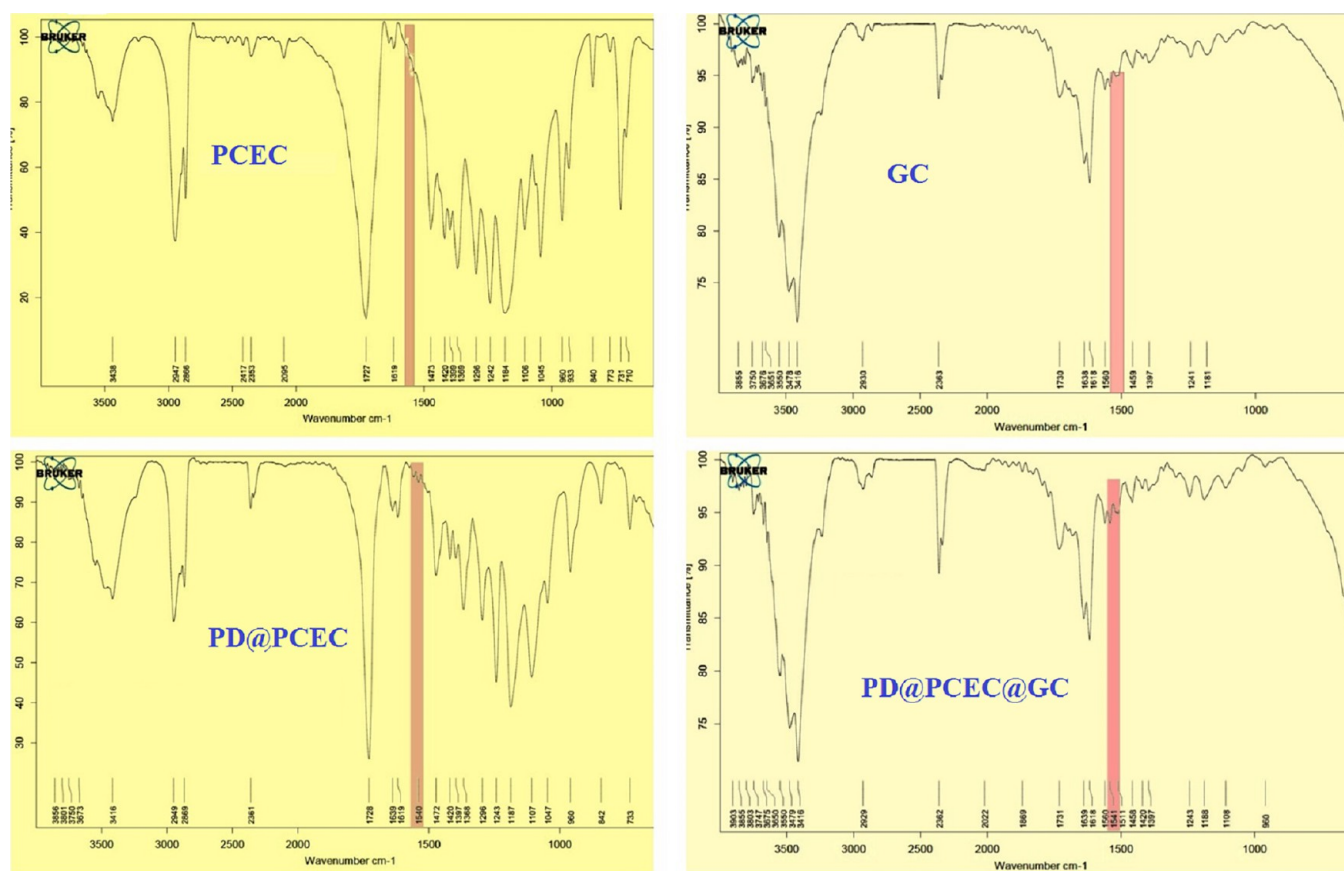
Figure 6. Comparison of FTIR spectra of PD@PCEC nanoparticles and scaffolds with and without encapsulated PDGF-BB.

Figure 5c illustrates the XRD patterns produced with PCL, PEG, and PD@PCEC nanospheres. The XRD pattern of the PCEC copolymer combines the crystalline peaks of pure PCL ($2\theta = 21.7°$ and $2\theta = 24.8°$) and pure PEG4000 ($2\theta = 19.3°$ and 23.9°). It exhibits three diffraction peaks at $2\theta = 19.3°$, $2\theta = 21.7°$, and $2\theta = 23.7°$. These findings are consistent those of prior studies.[63,64] The obtained results demonstrate that the blocks in the PCEC copolymer have the same crystalline structures as the parent homopolymers but with reduced crystallinity.

Along with the EE measurement, it was fascinating to examine the microscopic images of the resulting nanospheres. PD@PCEC nanospheres had a spherical form and a smooth surface (7a), with a diameter range of 72.3−344 nm (Figure 7b). SEM images of the GC and PD@PCEC@GC scaffolds are presented in Figure 7c and d, respectively. The images show that the scaffolds have a porous structure with interconnected pores, which is important for cell adhesion, proliferation, and tissue regeneration.

From the SEM images of the scaffolds with and without dispersed nanospheres, it can be concluded that both scaffolds have suitable porosity for use in cell culture (Figure 7c,d). The mean pore size of each scaffold was determined using ImageJ software (NIH, USA). The average pore size of the GC scaffold was 100 ± 36 μm, and it was lower and equal to 70.0 ± 17 μm for the PD@PCEC@GC scaffold.

The mechanical properties of scaffolds play a crucial role in tissue engineering, especially in applications such as wound dressings. The Young's modulus of the scaffolds was tailored to approximate the elasticity of human skin, with the PD@PCEC@GC scaffold showing a higher modulus than the GC scaffold after the addition of nanospheres. This increase in strength is important for maintaining the scaffold's structural integrity during use. Young's modulus of the GC scaffold made in this project was set at approximately 640 kPa. This value increased to 771 kPa after the addition of nanospheres to the scaffold structure.

By comparison of the GC scaffold and the PD@PCEC@GC scaffold, it was observed that the porosity of the latter is about 19% lower than that of the scaffold without nanospheres (Figure 7f). This observation can be explained by the occupation of a part of the pores of the GC scaffold by nanospheres. Nevertheless, it seems that the scaffold structure with nanospheres is still suitable for mimicking the epithelial tissue ECM in terms of porosity and pore size.

The swelling behavior of the scaffolds in PBS solution is essential for their functionality as wound dressings. The controlled swelling capacity of the scaffolds, as observed in Figure 8b, ensures that they can absorb biological fluids without rapid degradation. This property is critical for maintaining the scaffold's structural integrity over an extended period, which is essential for wound healing applications. The swelling of our scaffolds increased up to 96 h. Then, it reached an almost constant value. By comparison of the GC and PD@PCEC@GC scaffolds, it can be seen that the addition of PD@PCEC nanospheres to the structure of the GC scaffold reduces its swelling capacity in PBS solution. Because some of the pores of the hydrophilic GC scaffold are occupied by these amphiphilic nanospheres, the penetration of the solvent into them is less and the space required for the swelling of gelatin and collagen polymer strands is reduced. The maximum
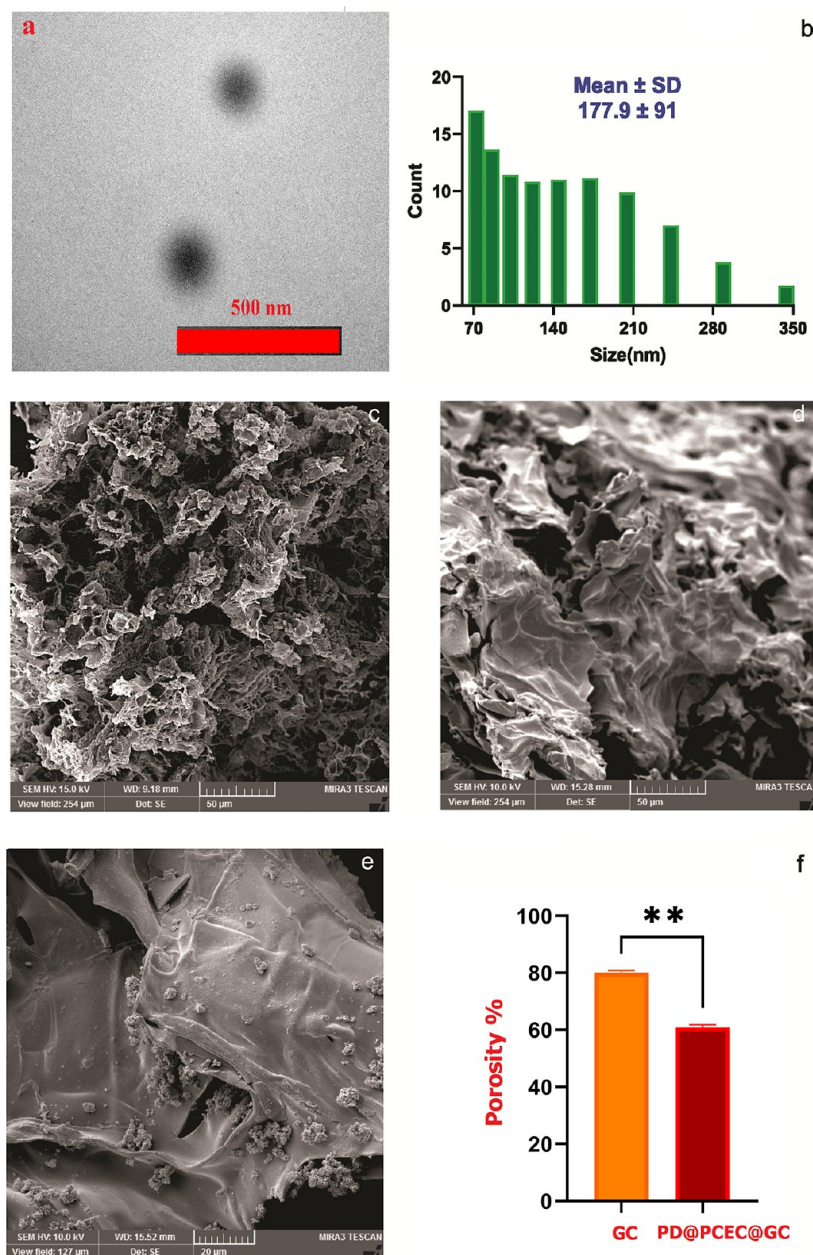
Figure 7. (a) Transmission electron microscopy (TEM) micrograph of the PD@PCEC nanospheres. (b) Size distribution of the nanospheres. The majority of the nanospheres are in the range of 100−160 nm. Scanning electron microscopy (SEM) micrographs of the (c) GC and (d) PD@PCEC@GC scaffolds for morphological analysis. (e) Scanning electron microscopy (SEM) micrograph of the ADSCs on the PD@PCEC@GC scaffold. (f) Comparison of GC and PD@PCEC@GC scaffold porosity.

swelling ratio was 20.1 in the GC scaffold and 11 in the PD@PCEC@GC scaffold.

The degradation rate of scaffolds depends on the composition of their components and the number of voids in which they are designed. For the suitable release of the growth factor from the scaffold, the porous structure of the scaffold and its stability in biological fluids should be adjusted. Owing to the hydrophilic nature of the GC hydrogel and the appropriate cross-link percentage, the growth factor was released almost 2% lower than that of PD@PCEC nanospheres. The release did not occur immediately and in a high amount. Compared with copolymers with more hydrophilicity, the PCEC copolymer is degraded at a slower rate, which may explain the slower and continuous growth factor release.

Figure 8c,d shows the scaffold degradation process over 21 days in PBS solution and the scaffold enzymatic degradation process over 8 h. As expected, degradation of the scaffolds in the presence of PBS solution containing enzyme occurs much faster than degradation in PBS solution without enzyme (8 h compared to 21 days).[65] The enzyme destroys the protein structure of collagen and gelatin. The results showed that the PD@PCEC@GC scaffold in PBS solution at pH 7.4 degraded to 36% ($w_t - w_t$) in 7 days, to 47% in 14 days, and to 54% in 21 days. The degradation rate of the GC in the presence of the lysozyme enzyme, the scaffolds degraded much faster, with a degradation rate of approximately 60% after 8 h, and no significant difference was observed between the speed of degradation of the GC and PD@PCEC@GC scaffolds because the enzyme is fast in dividing protein strands. The
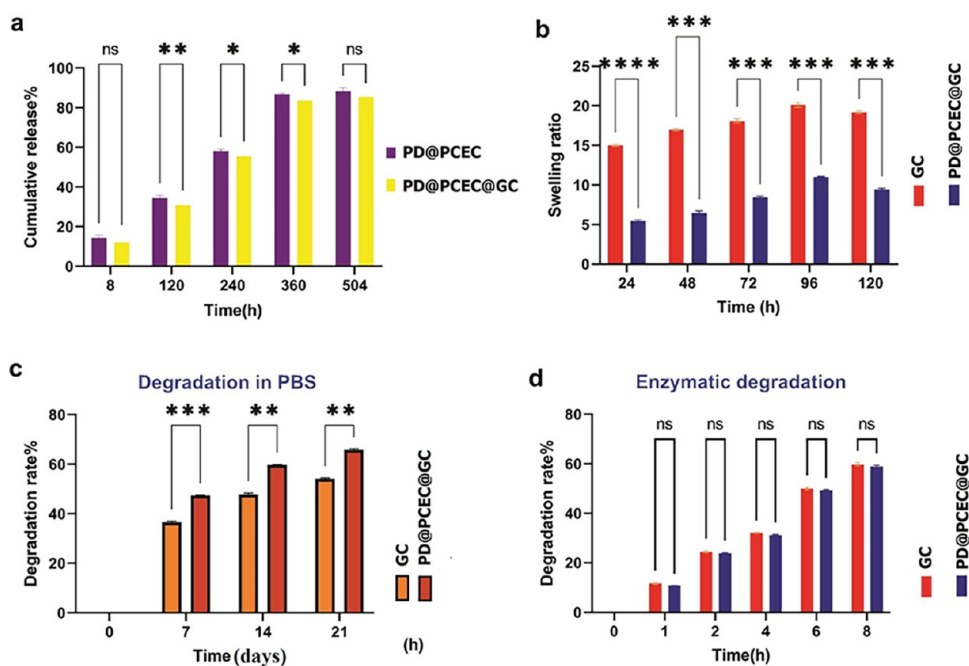
Figure 8. (a) Release profiles of the PDGF-BB from the PDGF-BB-loaded PD@PCEC nanospheres and PD@PCEC@GC scaffold as determined by the ELISA assay. The data was expressed as means ± SD ($n = 3$). (b) Swelling behavior of the scaffolds in PBS (at pH = 7.4, 37 °C), for 120 h. (c) The degradation profile of the GC and PD@PCEC@GC hydrogels in PBS (at pH = 7.4, 37 °C), and during 21 days. The medium was replaced with a fresh medium every 3 days. (d) The degradation profile of the GC, and PD@PCEC@GC hydrogels in PBS solution containing 13 mg/liter of lysozyme at 37 °C (*$p < 0.05$, **$p < 0.01$, ***$p < 0.001$, ****$p < 0.0001$, and ns means there is no significant difference).

physicochemical properties of the prepared scaffolds are summarized in Table 5.

Table 5. Scaffold Physiochemical Properties

	GC scaffold	PD@PCEC@GC scaffold
porosity %	80.0	61.0
pore size (μm)	100 ± 36	70.0 ± 17
Young's modulus (kPa)	640	771
swelling ratio	17.9	8.18

3.3. Investigation of PDGF-BB Release. The sustained release of PDGF-BB from PD@PCEC nanospheres and PD@PCEC@GC scaffolds is a crucial aspect of their potential applications in tissue engineering. The release profile showed that approximately 85% of the loaded PDGF-BB was released from the nanospheres during the first 360 h, with a sustained release over the entire 504 h period (Figure 8a). The PDGF-BB release profile revealed that the strategy used to control the release from nanospheres and the PD@PCEC@GC scaffold in this investigation was adequate and could be used in future studies.

3.4. Bioactivity Assay of the Released PDGF-BB. As shown in Figure 9a, the bioactivity of released PDGF-BB was 87.3%. The released PDGF-BB retained its bioactivity, as evidenced by its ability to stimulate the proliferation of HGFCs. This indicates that the biological structure of PDGF is preserved in this scaffold, and only a small amount is lost during release. Therefore, it can be concluded that this encapsulation method is efficient for the regular and gradual release of PDGF-BB from PD@PCEC nanospheres.

3.5. In Vitro Study. In this study, hADSCs were cultured on each scaffold, the MTT test determined their proliferation and viability, and their differentiation into keratinocyte-like
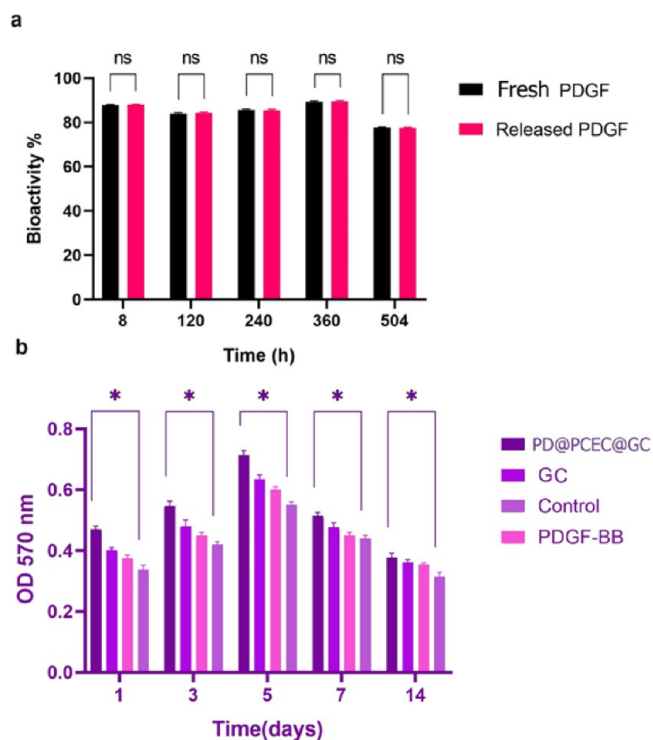
Figure 9. (a) Released PDGF-BB bioactivity based on cellular proliferation. (b) MTT assay results for hADSCs cultured on PD@PCEC@GC and GC scaffolds and cultured in the presence of PDGF-BB for 1, 3, 5, 7, and 14 days (*$p < 0.05$, and ns means there is no significant difference).

cells were confirmed by microscopic observation, RT-PCR, and Western blot analysis
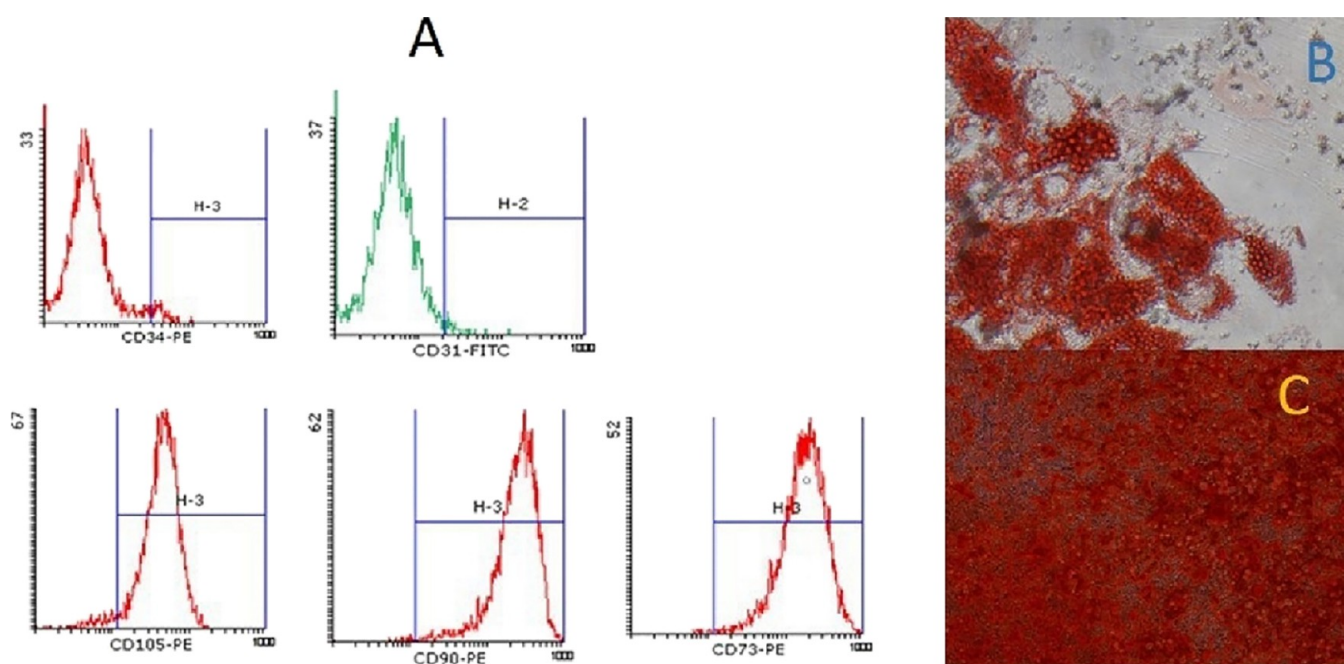
Figure 10. Assessment of the differentiation potential in hADSCs. (A) Flow cytometry analysis for surface markers CD34, CD31, CD105, CD90, and CD73. (B) Adipogenic differentiation was shown by Oil Red O, which stained the fat vacuoles inside the cytoplasm. (C) By staining Alizarin Red S, mineralization following osteogenic differentiation was visualized.

3.5.1. Characterization of hADSCs. After recovery from thawing, frozen hADSCs from P3 adhered to flasks and gained >90% confluence within 3 days of cultivation in DMEM/F12. As shown in Figure 11 (control group), the cells have a spindle-like morphology and can be arranged into a whirlpool. The hADSCs expressed CD90, CD73, and CD105 on their cell surfaces, but neither CD34 nor CD33 (Figure 10A) were significantly expressed.[66] After adipogenic and osteogenic medium cultivation, Oil Red O and Alizarin Red stain revealed differentiation into adipocytes and osteoblasts with matrix mineralization (Figures 106C and 10).

3.5.2. In Vitro Cell Attachment and Proliferation. In Figure 7e, adherent ADSCs can be observed on the surface of the PD@PCEC@GC scaffold. Figure 9b shows that cell viability increases with time up to the fifth day of the culture. The growth and proliferation of cells decreased, but the viability of cells was significantly higher than in the control group. Compared with the control group, all scaffolds induced hADSC proliferation, and all scaffold groups had greater than 100% cell viability. In PD@PCEC@GC, GC scaffolds, and in the presence of PDGF-BB, cell viability was significantly higher than that in the control group ($P < 0.05$). PD@PCEC nanospheres promote cell proliferation continuously by releasing growth factors. The MTT assay showed that PDGF-BB enhanced cell proliferation when incorporated into the PD@PCEC@GC. Based on the biocompatibility test, PDGF-BB can promote cell survival in skin tissue engineering.[8,67] Overall, all scaffolds are treated as biocompatible with the cells.

3.5.3. Microscopic Observation Using a Light Microscope. Microscopic observation of attached cells in culture flasks at specified intervals revealed that in the differentiation group with ATRA, the morphology of the cells changed from spindle-shaped to rounded/polygonal on the seventh day. However, this morphological change in the differentiation group with PDGF-BB (PD@PCEC@GC group) occurred a little late and

occurred on the 10th day. The differentiation group with ATRA (PD@PCEC@GC + ATRA group) showed a higher presence of circularly shaped cells than the PD@PCEC@GC group. On the 14th day, most of the stem cells cultured on the scaffolds were circular/polygonal. On the 21st day and the final evaluation of the cells under the microscope, the formation of multiple clusters was observed (11). Additionally, in the differentiation group with ATRA, presumably due to the presence of a minor amount of DMSO in the culture medium
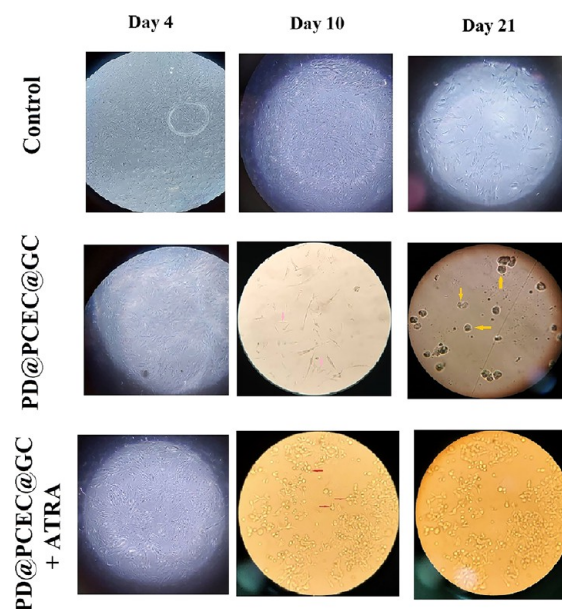
Figure 11. hADSC morphology under a light microscope: (A) following 4 days of culture on the PD@PCEC@GC hydrogels, (B) following 10 days of culture on the PD@PCEC@GC hydrogels, and (C) following 21 days of cultured on the PD@PCEC@GC hydrogels.
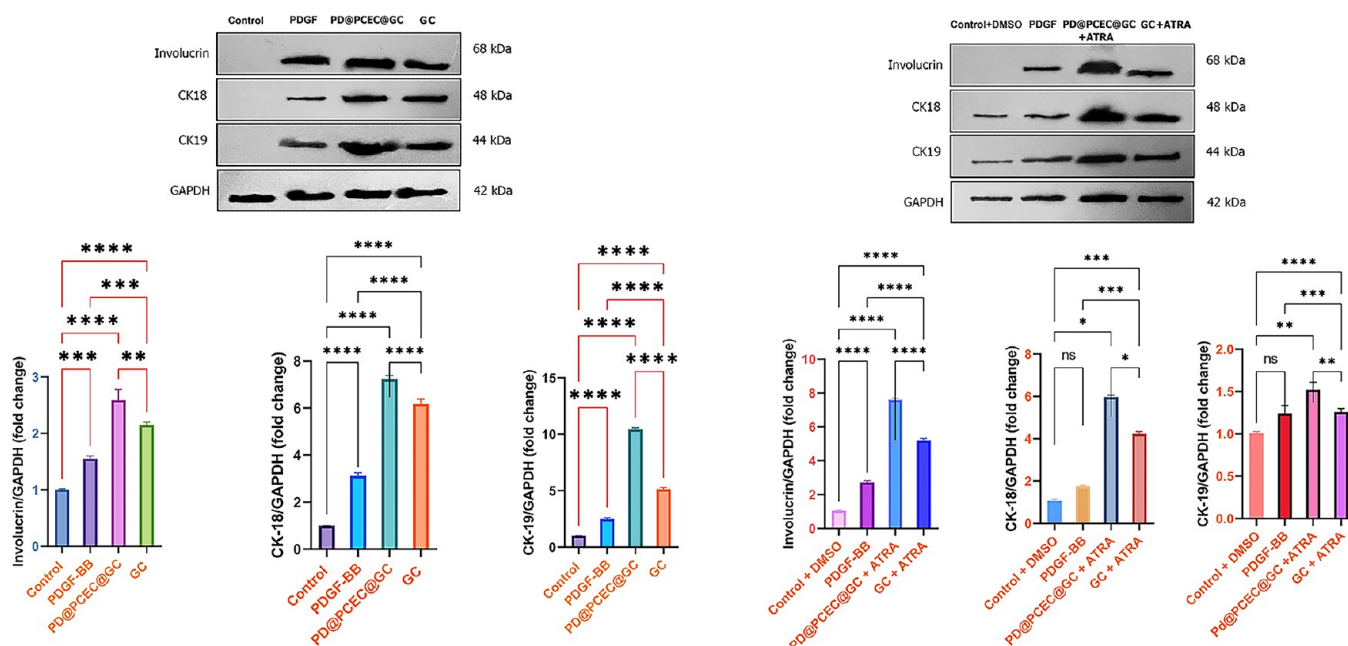
Figure 12. Representative Western blots of hADSCs cultivated in DMEM/F12 media on scaffolds in comparison to control samples (hADSCs cultivated in two flasks in DMEM/F12 media with and without adding of DMSO) showing the expression of involucrin (68 kDa), CK-18 (48 kDa), and CK-19 (44 kDa); corresponding GAPDH (42 kDa) was used as loading control.

compared with the first control group, slight alterations in the morphology of the ADSCs were observed on the third day of cell culture.

3.5.4. Western Blotting.
For the convenience of data analysis and to facilitate data comparison, the samples were divided into two main groups: the ATRA- and non-ATRA-differentiated groups. Within the non-ATRA-differentiated group, the following subgroups were identified: the control group without DMSO, the PDGF group, the GC group, and the PD@PCEC@GC group. In the ATRA-differentiated group, in addition to the control group with DMSO, there were supplementary subgroups: the PDGF group, the GC group along with ATRA, and the PD@PCEC@GC group along with ATRA (Figure 12).

Western blot analysis revealed that both CK-18 and CK-19 were expressed in the control group, where stem cells were cultured in DMEM/F12 with a small amount of DMSO. However, in the control group without DMSO, the expression of these two genes was not significant (Figure 12). This situation was observed both in the RT-PCR test and in the Western blot. Involucrin was not expressed in any of the control groups. However, it was expressed in the groups of differentiated cells with ATRA and the group of differentiated cells with the growth factor released from the PD@PCEC@GC scaffold. This confirms the differentiation of the cells into keratinocyte-like cells in these groups. The upregulation levels of CK-18 and CK-19 in the PDGF group were greater than those of differentiated cells in the ATRA group, indicating that PDGF-BB enhances hADSC keratinocyte-like cell differentiation more effectively.

3.5.5. RT-PCR for Keratinocyte-Specific Gene Expression.
RT-PCR analysis was performed to evaluate the expression of keratinocyte-specific genes in the different groups. The expression levels of CK-18, CK-19, and involucrin were significantly higher in differentiated cells in all groups than in undifferentiated hADSCs (control and control + DMSO

groups). The upregulation levels of CK-18 and CK-19 (6.90-fold, $p < 0.001$, for CK-18, 10.4-fold, $p < 0.001$, for CK-19) in the non-ATRA-differentiated group were higher than those (1.80-fold, $p < 0.01$ for CK-18, 1.45-fold, $p < 0.001$ for CK-19) in the ATRA-differentiated group. In comparison, the upregulation level of involucrin in the ATRA-differentiated group was higher (8.50 folds, $p < 0.001$) than that in the non-ATRA-differentiated group (2.30 folds, $p < 0.001$).

This feature article addresses the impact of PDGF-BB keratinocyte differentiation. The effect of ATRA is clearly defined by comparing the results of investigating the expression of involucrin in the presence and absence of ATRA. By increasing the speed and rate of ADSC differentiation into keratinocytes, ATRA increases the level of involucrin expression. In this way, the amount of this expression in the ATRA group was almost twice that in the group without ATRA.

On the other hand, as can be seen in Figure 13, in both differentiation groups, the expression levels of CK-18, CK-19, and involucrin in the PD@PCEC@GC scaffold are higher than those in the GC scaffold, and that is higher than the expression levels of these genes in differentiated stem cells in cell culture flasks and the presence of PDGF.

4. DISCUSSION
The skin is the first defense barrier of the human body against the entry of pathogenic organisms and harmful rays and substances. Therefore, it is necessary to maintain its integrity to be as effective as possible. Wound healing is a regular and complex process in which various factors, such as cytokines and growth factors, stem cells, fibroblasts, and some vitamins, play an essential role in correctly implementing its steps. Inefficiency or a lack of any of these factors can disrupt wound healing and cause chronic wounds. One of the most common chronic wounds in humans are diabetic ulcers. Considering the increase in the prevalence of diabetic wounds worldwide and
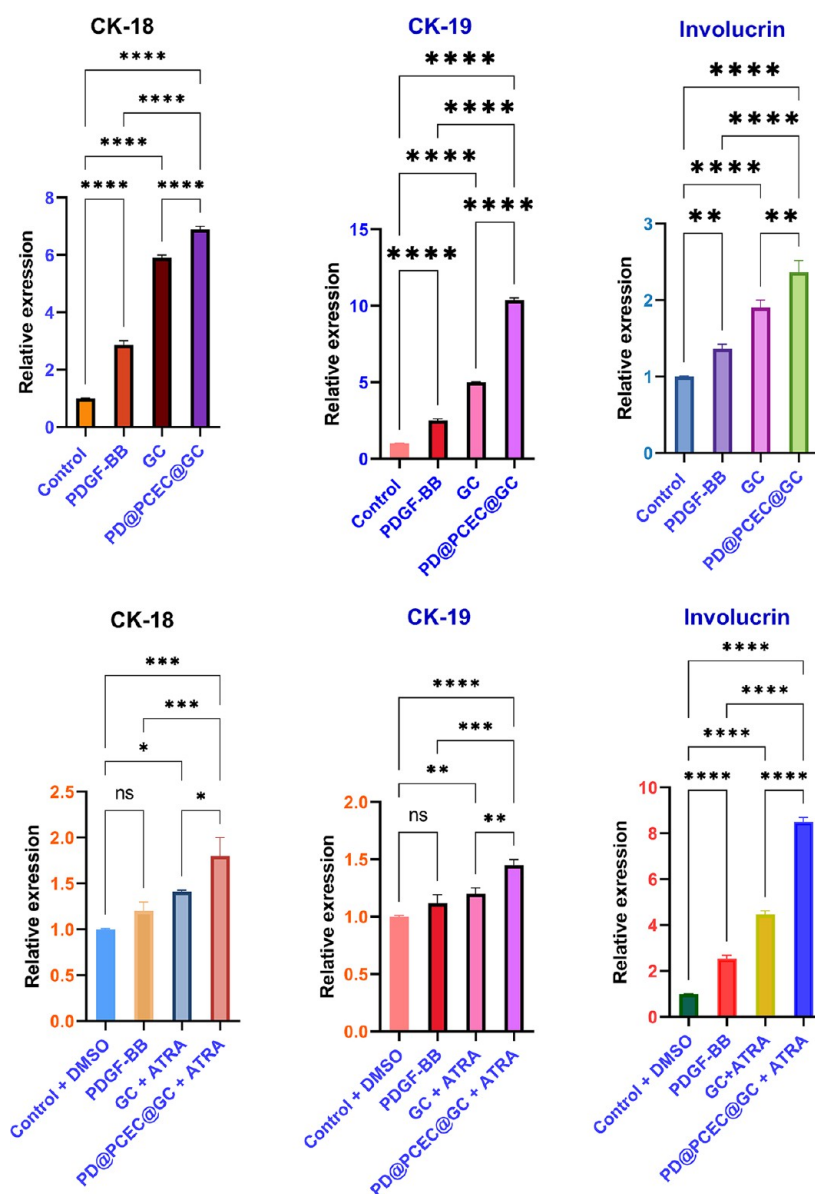
Figure 13. Expression of keratinocyte marker gene involucrin, CK-18, and CK-19 in hADSCs seeded on GC, and PD@PCEC@GC scaffolds, and cultured in flask in the presence of PDGF within 21 days by real-time PCR analysis (ns, no significant difference), $*p < 0.05$, $**p < 0.01$, $***p < 0.001$, and $****p < 0.0001$). To normalize the genes, GAPDH was used.

the need to speed up the healing of these wounds in patients to prevent amputation, it seems necessary to use newer and more effective wound dressings. The amount of platelet growth factor secreted in the blood of these patients during wound formation is less than that needed to start the healing process. Therefore, a biocompatible dressing that regularly and continuously releases this growth factor can solve this problem.

As mentioned earlier, mesenchymal stem cells play an essential role in wound healing. The most readily available cells for extraction and cultivation are mesenchymal stem cells derived from adipose tissue. These cells are pluripotent and can differentiate into various cell lines.

Considering all these materials, in this study, we prepared a hydrogel scaffold loaded with PDGF-BB-containing nanospheres and conducted a comprehensive characterization of nanospheres and scaffolds designed for potential applications in skin tissue engineering. The results of our characterization

efforts provide valuable insights into the suitability of these materials for various biomedical applications.

3D scaffolds, similar to the real ECM of tissues, can improve blood supply to cells and their viability.[68−70] Therefore, it is better to employ sponge-like scaffolds with sufficient pores to achieve this goal and create a platform similar to the extracellular matrix for cells. Various methods, such as applying porogens[71,72] and freeze-drying, are used to prepare scaffolds with the desired porosity.[73] Among these methods, freeze-drying is the easiest and most widely used. Therefore, this study used it to create a porosity in the synthesized scaffolds. SEM checked the structure of the prepared porous scaffold to ensure appropriate porosity and pore size. Porous and three-dimensional structures of GC enable the most effective implantation of cells on the surface and inside cavities and their differentiation into more specialized cells.[74] In some other studies on the differentiation of stem cells into keratinocytes on porous scaffolds, the size of the pores of

the scaffolds was similar to that of the scaffold prepared in this project.[15,45]

According to research conducted by Agache et al., as a person ages, the skin's elasticity decreases, and as a result, its Young's modulus increases. The Young's modulus of the skin of people under 30 is about 420 kPa; for people over 30 years old, it is about 850 kPa.[75] Therefore, to mimic skin elasticity, scaffold Young's modulus should be brought close to human skin's Young's modulus by appropriate cross-linking. Hydrogels made for stem cell differentiation into skin cells must have the same mechanical properties as those of the skin. In addition, they must have hydrophilicity, porosity, and proper strength.[76] The mechanical properties and Young's modulus of the scaffolds prepared in this study are comparable to those of scaffolds prepared by other researchers for skin reconstruction.[77−79] As observed in the investigation of scaffold structure degradation, the scaffold strength increases after the addition of nanospheres. According to the compressive modulus results, the PD@PCEC@GC scaffold is a suitable option for human skin tissue engineering.

Adherent cells, such as mesenchymal cells, require proper connections with their neighboring cells for growth and proliferation.[80] The porosity of the scaffold used for the proliferation and differentiation of stem cells plays an essential role in the survival rate. In addition, it facilitates effective communication between cells and aids in differentiating these cells into the desired cells. The proper size of the pores, shape, and connection of these pores in the three-dimensional structure of the scaffold helps to place the cells together.[81] By imitating the 3D structure of the epithelial tissue, it can guide the cells toward keratinocytes.

In six conducted studies in the years preceding, both natural and synthetic composite scaffolds have been employed for the cultivation and differentiation of stem cells into keratinocytes.[16,82−86] In none of these studies did researchers utilize growth factors released from the scaffold for the differentiation of stem cells. Instead, they emphasize the physicochemical properties of the scaffolds or the differentiation medium. Our study is similar to these six studies in employing biocompatible composite scaffolds for stem cell cultivation. The use of PDGF-BB for the differentiation of stem cells into keratinocytes has been conducted for the first time. Considering the insufficient secretion of this growth factor in diabetic patients and the delayed wound healing observed in these individuals, this study could serve as a potential breakthrough in accelerating the healing of cutaneous wounds in this patient population.

To function optimally as a wound dressing, the scaffold must be able to absorb water and biological fluids. Nevertheless, this absorptive capacity should not result in the scaffold's swift degradation over a brief period. For this purpose, hydrogels are more appropriate options, because of their network and hydrophilic nature. Collagen and gelatin, which are more similar to the natural ECM of epithelial tissue, are also well used for this purpose.[87−89] To increase the stability of the scaffolds while maintaining their hydrophilic nature, it is necessary to cross-link them with the necessary percentage and a suitable cross-linker. The degradation rate of scaffolds is a crucial factor in their suitability for tissue engineering. The controlled degradation of the PD@PCEC@GC scaffold in PBS solution and its accelerated degradation in the presence of a lysozyme enzyme demonstrate its potential for use in different biological environments. The slower degradation rate of the PD@PCEC@GC scaffold compared to the GC scaffold is

likely due to the occupation of scaffold pores by nanospheres, hindering solvent penetration and reducing overall degradation.

The investigation of PDGF-BB release is essential for understanding how the scaffolds can deliver growth factors to promote tissue regeneration. In earlier studies of continuous PDGF-BB release, the release period was typically brief,[90] or the release profile was initially associated with a burst release.[91−93] Prior studies have used PDGF-BB adsorption on biocompatible and biodegradable polymers to maintain and deliver PDGF-BB continuously. The same phenomenon probably causes the burst release of the growth factor during the first stage. Water infiltration into the pores carrying the growth factor leads to the rapid destruction of the scaffold. Our release system of PDGF-BB has the advantage of providing PDGF-BB without sudden release because of the biodegradable copolymer structure of PCEC. The release profile of PDGF-BB from our prepared nanospheres was uniform and obtained in 504 h. This controlled release ensures a continuous supply of PDGF-BB to the surrounding cells, promoting cell proliferation and tissue regeneration.

In a similar vein, Li and his colleagues developed a nanocomposite hydrogel containing synthetic magnesium silicate clay that gradually releases PDGF-BB. Despite the regular and gradual release profile, more than 60% of the growth factor is released within the first 5 days.[94] In contrast, our scaffold releases a comparable amount of growth factor within 10 days, making it available for cell differentiation into keratinocytes. Additionally, Wei et al. utilized a PLGA copolymer to encapsulate platelet growth factor and the PDGF-BB-release profile of these polymer microspheres was also favorable.[95] Combining the results of this research with our work, it can be concluded that encapsulation in a biocompatible synthetic polymer is a superior method for achieving continuous PDGF-BB release. The bioactivity assay conducted on the released PDGF-BB offers a critical perspective on the practical implications of our scaffold in the context of tissue engineering and wound healing. Maintaining the bioactivity of growth factors, such as PDGF-BB, during release is crucial, as it directly influences their effectiveness in promoting cellular responses. Our results demonstrate that the released PDGF-BB retained an impressive bioactivity level of approximately 87.3%. This finding implies that the biological structure of PDGF-BB remains intact throughout the release process. More importantly, the preserved bioactivity signifies that the growth factor can effectively stimulate the proliferation of HGFCs. This outcome has profound implications for clinical applications of our scaffold. The controlled and efficient release of PDGF-BB from the scaffold enhances its therapeutic potential and makes it a promising candidate for clinical use in regenerative medicine. However, further in vivo studies and clinical trials are required to fully validate its efficacy and safety in human applications.

Our in vitro study centered on the cultivation of hADSCs on the developed scaffolds and their subsequent assessment for proliferation, viability, and differentiation into keratinocyte-like cells. The hADSCs exhibited favorable characteristics, including adherence, proliferation, and morphological changes indicative of differentiation into keratinocyte-like cells. These findings align with previous studies that have underscored the adaptability of ADSCs for regenerative applications in skin tissue engineering.[96−98] The scaffold's role in facilitating cell

attachment, viability, and proliferation is pivotal for its success in tissue engineering. The high cell viability observed in the MTT assay indicates excellent biocompatibility and low cytotoxicity, essential for maintaining a conductive environment for cell growth and tissue regeneration. Moreover, the observed morphological transformations following cell differentiation support the suitability of the PD@PCEC@GC scaffold for the phenotypic induction of keratinocytes in vitro. It is worth noting that the addition of PDGF-BB further enhanced the scaffold's potential to induce keratinocyte-specific gene expression, including CK-18, CK-19, and involucrin.

Gelatin-collagen scaffolds, because of the presence of amino and acidic functional groups along their proteinaceous chains, can establish bonds with integrins present on the surface of ADSCs. This enables these scaffolds to effectively adhere cellular entities to their surface. The adherence of cells to scaffolds leads to their proximity and facilitates effective intercellular communication, thereby fostering cell proliferation and growth.

Cell morphology varies across tissues, with different shapes and structures serving specific functions. For instance, epithelial cells are flat and polygonal for barrier and absorption roles while muscle cells are elongated for contraction. In contrast, ADSCs change from a fibroblast-like spindle shape to a flattened, polygonal form when differentiating into keratinocyte-like cells, acquiring keratin filaments and specialized features. This transformation highlights ADSCs' adaptability for regenerative applications in skin tissue engineering and wound healing. The morphological changes observed in our study, following the differentiation of stem cells into keratinocytes, were consistent with previous studies[99−101] in this field and were well-documented under the microscope. In the further differentiation evaluation using RT-PCR and Western blotting, the expression of Ck-18 and Ck-19 in the control group with DMSO can be attributed to the presence of DMSO in the culture medium. This suggests that DMSO may act as an inducer of the differentiation of mesenchymal stem cells into hepatocytes, and hepatocytes also express CK-18 and CK-19 genes, as observed in previous studies.[102,103] Our findings documented that the PD@PCEC@GC scaffold could work as an appropriate matrix for enhancing keratinocyte commitment of hADSCs. However, the major limitation of the study is storage and freezing of KLCs grown on the PD@PCEC@GC scaffold for future clinical applications, which should be optimized in upcoming complementary studies.

5. CONCLUSIONS

The results of this project showed that gel-cold hydrogel dressings with encapsulated PDGF-BB promoted the proliferation and viability of hADSCs in vitro. The release of PDGF-BB from the PD@PCEC nanospheres in the PD@PCEC@GC scaffold was controlled and sustained for over 504 h, providing a continuous and gradual supply of the growth factor to support cell proliferation and differentiation. The PD@PCEC@GC scaffold demonstrated suitable porosity, mechanical properties, and biocompatibility for cell attachment, growth, and desirable responses. Adding PD@PCEC nanospheres to the GC scaffold enhanced its mechanical strength, making it a promising option for future tissue engineering. After observing the morphological changes of the cells under the microscope and performing RT-PCR and

Western blot tests, we concluded that the PD@PCEC@GC scaffold would be an appropriate matrix for in vitro keratinocyte phenotypic induction. In addition, the synthesized scaffolds stimulated hADSC differentiation and the addition of PDGF-BB enhanced the keratogenic capacity of the PD@PCEC@GC hydrogel by inducing CK-18, CK-19, and involucrin. The findings of this investigation may support the development of proper matrix for ADSCs toward skin regeneration and wound dressing.

■ AUTHOR INFORMATION

Corresponding Authors

Effat Alizadeh − *Department of Medical Biotechnology, Faculty of Advanced Medical Sciences, Tabriz University of Medical Sciences, Tabriz 51664-15731, Iran;* Phone: +984133341933; Email: e.alizadeh.2010@gmail.com, alizadehe@Tbzmed.ac.ir

Soodabeh Davaran − *Department of Medicinal Chemistry, Faculty of Pharmacy, Tabriz University of Medical Sciences, Tabriz 51664-14766, Iran; Research Center for Pharmaceutical Nanotechnology, Biomedicine Institute, Tabriz University of Medical Sciences, Tabriz 51664, Iran;* Phone: +984131772333; Email: S.davaran2018@gmail.com, Davaran@Tbzmed.ac.ir

Authors

Raheleh Hazrati − *Department of Medicinal Chemistry, Faculty of Pharmacy, Tabriz University of Medical Sciences, Tabriz 51664-14766, Iran; Research Center for Pharmaceutical Nanotechnology, Biomedicine Institute, Tabriz University of Medical Sciences, Tabriz 51664, Iran;* orcid.org/0000-0001-9509-9688

Somaieh Soltani − *Department of Medicinal Chemistry, Faculty of Pharmacy, Tabriz University of Medical Sciences, Tabriz 51664-14766, Iran*

Peyman Keyhanvar − *Department of Medical Biotechnology, Faculty of Advanced Medical Sciences, Tabriz University of Medical Sciences, Tabriz 51664-15731, Iran*

Complete contact information is available at:
https://pubs.acs.org/10.1021/acsomega.3c09391

Author Contributions

R.H.: conceptualization, methodology, software, data curation, writing—original draft preparation. E.A.: supervision, methodology, review and editing. S.S.: reviewing and rditing. P.K.: reviewing. S.D.: data curation, visualization, methodology, supervision.

Notes

The authors declare no competing financial interest.
The study was approved by the Ethics Committee of Tabriz University of Medical Sciences, Tabriz, Iran. Ethics code was IR.TBZMED.VCR.REC.1397.123.

role in the design of the study and collection, analysis, and interpretation of data and in writing the manuscript.

■ REFERENCES

(1) Jari Litany, R. I.; Praseetha, P. K. Tiny tots for a big-league in wound repair: Tools for tissue regeneration by nanotechniques of today. *J. Controlled Release* **2022**, *349*, 443−459.

(2) Castellano-Pellicena, I.; Thornton, M. J. Isolation of Epidermal Keratinocytes from Human Skin: The Scratch-Wound Assay for Assessment of Epidermal Keratinocyte Migration. *Methods Mol. Biol.* **2020**, *2154*, 1−12.

(3) Schneider, I.; Calcagni, M.; Buschmann, J. Adipose-derived stem cells applied in skin diseases, wound healing and skin defects: a review. *Cytotherapy* **2023**, *25* (2), 105−119.

(4) Al-Ghadban, S.; Artiles, M.; Bunnell, B. A. Adipose stem cells in regenerative medicine: looking forward. *Front. Bioeng. Biotechnol.* **2022**, *9*, 1486.

(5) Alonso-Goulart, V.; Carvalho, L. N.; Marinho, A. L. G.; de Oliveira Souza, B. L.; de Aquino Pinto Palis, G.; Lage, H. G. D.; de Lima, I. L.; Guimarães, L. D.; Peres, L. C.; Silveira, M. M.; Lopes, G. H. N. L.; Ferreira, L. B.; de Souza Castro-Filice, L. Biomaterials and Adipose-Derived Mesenchymal Stem Cells for Regenerative Medicine: A Systematic Review. *Materials* **2021**, *14* (16), 4641.

(6) Mazini, L.; Rochette, L.; Admou, B.; Amal, S.; Malka, G. Hopes and Limits of Adipose-Derived Stem Cells (ADSCs) and Mesenchymal Stem Cells (MSCs) in Wound Healing. *International Journal of Molecular Sciences* **2020**, *21* (4), 1306.

(7) Si, Z.; Wang, X.; Sun, C.; Kang, Y.; Xu, J.; Wang, X.; Hui, Y. Adipose-derived stem cells: Sources, potency, and implications for regenerative therapies. *Biomed Pharmacother* **2019**, *114*, No. 108765.

(8) Dehkordi, A. N.; Babaheydari, F. M.; Chehelgerdi, M.; Dehkordi, S. R. Skin tissue engineering: wound healing based on stem-cell-based therapeutic strategies. *Stem Cell Res. Ther.* **2019**, *10* (1), 111.

(9) Ehnert, S.; Glanemann, M.; Schmitt, A.; Vogt, S.; Shanny, N.; Nussler, N. C.; Stöckle, U.; Nussler, A. The possible use of stem cells in regenerative medicine: dream or reality? *Langenbecks Arch Surg* **2009**, *394* (6), 985−97.

(10) Shokravi, S.; Borisov, V.; Zaman, B. A.; Niazvand, F.; Hazrati, R.; Khah, M. M.; Thangavelu, L.; Marzban, S.; Sohrabi, A.; Zamani, A. Mesenchymal stromal cells (MSCs) and their exosome in acute liver failure (ALF): a comprehensive review. *Stem Cell Res. Ther.* **2022**, *13* (1), 1−21.

(11) Hazrati, R.; Davaran, S.; Keyhanvar, P.; Soltani, S.; Alizadeh, E. A Systematic Review of Stem Cell Differentiation into Keratinocytes for Regenerative Applications. *Stem Cell Rev. Rep.* **2023**, *20*, 362−393.

(12) Abbasi, K.; Tavakolizadeh, S.; Hadi, A.; Hosseini, M.; Soufdoost, R. S.; Heboyan, A.; Alam, M.; Fani-Hanifeh, S. The wound healing effect of collagen/adipose-derived stem cells (ADSCs) hydrogel: In vivo study. *Veterinary Medicine and Science* **2023**, *9* (1), 282−289.

(13) Guo, X.; Schaudinn, C.; Blume-Peytavi, U.; Vogt, A.; Rancan, F. Effects of Adipose-Derived Stem Cells and Their Conditioned Medium in a Human Ex Vivo Wound Model. *Cells* **2022**, *11* (7), 1198 DOI: 10.3390/cells11071198.

(14) Fukui, E.; Funaki, S.; Kimura, K.; Momozane, T.; Kimura, A.; Chijimatsu, R.; Kanzaki, R.; Kanou, T.; Ose, N.; Minami, M.; Miyagawa, S.; Sawa, Y.; Okumura, M.; Shintani, Y. Adipose Tissue-Derived Stem Cells Have the Ability to Differentiate into Alveolar Epithelial Cells and Ameliorate Lung Injury Caused by Elastase-Induced Emphysema in Mice. *Stem Cells Int.* **2019**, *2019*, 5179172.

(15) Pilehvar-Soltanahmadi, Y.; Nouri, M.; Martino, M. M.; Fattahi, A.; Alizadeh, E.; Darabi, M.; Rahmati-Yamchi, M.; Zarghami, N. Cytoprotection, proliferation and epidermal differentiation of adipose tissue-derived stem cells on emu oil based electrospun nanofibrous mat. *Exp. Cell Res.* **2017**, *357* (2), 192−201.

(16) Bayati, V.; Abbaspour, M. R.; Dehbashi, F. N.; Neisi, N.; Hashemitabar, M. A dermal equivalent developed from adipose-derived stem cells and electrospun polycaprolactone matrix: an in vitro and in vivo study. *Anat Sci. Int.* **2017**, *92* (4), 509−520.

(17) Yan, Y.; Liu, Y.; Liu, D.; He, L.; Guan, L.; Wang, Y.; Nan, X.; Pei, X. Differentiation of adipose-derived adult stem cells into epithelial-like stem cells. *Ann. Anat* **2013**, *195* (3), 212−8.

(18) Li, H.; Xu, Y.; Fu, Q.; Li, C. Effects of multiple agents on epithelial differentiation of rabbit adipose-derived stem cells in 3D culture. *Tissue Eng. Part A* **2012**, *18* (17−18), 1760−70.

(19) Heldin, C. H.; Westermark, B. Platelet-derived growth factor: mechanism of action and possible in vivo function. *Cell Regul* **1990**, *1* (8), 555−66.

(20) Lee, S. J. Cytokine delivery and tissue engineering. *Yonsei Med. J.* **2000**, *41* (6), 704−19.

(21) Saik, J. E.; Gould, D. J.; Watkins, E. M.; Dickinson, M. E.; West, J. L. Covalently immobilized platelet-derived growth factor-BB promotes angiogenesis in biomimetic poly(ethylene glycol) hydrogels. *Acta Biomater* **2011**, *7* (1), 133−43.

(22) Manjili, H. K.; Sharafi, A.; Danafar, H.; Hosseini, M.; Ramazani, A.; Ghasemi, M. H. Poly(caprolactone)−poly(ethylene glycol)−poly(caprolactone) (PCL−PEG−PCL) nanoparticles: a valuable and efficient system for in vitro and in vivo delivery of curcumin. *RSC Adv.* **2016**, *6* (17), 14403−14415.

(23) Eatemadi, A.; Daraee, H.; Aiyelabegan, H. T.; Negahdari, B.; Rajeian, B.; Zarghami, N. Synthesis and Characterization of Chrysin-loaded PCL-PEG-PCL nanoparticle and its effect on breast cancer cell line. *Biomed Pharmacother* **2016**, *84*, 1915−1922.

(24) Alami-Milani, M.; Zakeri-Milani, P.; Valizadeh, H.; Salehi, R.; Jelvehgari, M. Preparation and evaluation of PCL-PEG-PCL micelles as potential nanocarriers for ocular delivery of dexamethasone. *Iran J. Basic Med. Sci.* **2018**, *21* (2), 153−164.

(25) Jahangiri, S.; Amirkhani, L.; Akbarzadeh, A.; Hajimohammadi, R. Encapsulation of Doxorubicin and Chrysin on magnetic PCLPEG-PCL nanoparticles: Optimization of parameters and drug delivery evaluation. *Int. J. Nano Dimens.* **2021**, *12* (4), 380−392.

(26) Hu, C.; Chen, Z.; Wu, S.; Han, Y.; Wang, H.; Sun, H.; Kong, D.; Leng, X.; Wang, C.; Zhang, L.; Zhu, D. Micelle or polymersome formation by PCL-PEG-PCL copolymers as drug delivery systems. *Chin. Chem. Lett.* **2017**, *28* (9), 1905−1909.

(27) Gökçe Kocabay, Ö.; İsmail, O. Preparation and optimization of biodegradable self-assembled PCL-PEG-PCL nano-sized micelles for drug delivery systems. *International Journal of Polymeric Materials and Polymeric Biomaterials* **2021**, *70* (5), 328−337.

(28) du Toit, L. C.; Choonara, Y. E.; Pillay, V. An Injectable Nano-Enabled Thermogel to Attain Controlled Delivery of p11 Peptide for the Potential Treatment of Ocular Angiogenic Disorders of the Posterior Segment. *Pharmaceutics* **2021**, *13* (2), 176.

(29) Choi, J.; Pant, A.; Medikonda, R.; Kim, Y.-H.; Routkevitch, D.; Saleh, L.; Tong, L.; Chan, H. Y.; Nedrow, J.; Jackson, C.; Jackson, C.; Lim, M. Sustained localized delivery of immunotherapy to lymph nodes reverses immunosuppression and increases long-term survival in murine glioblastoma. *OncoImmunology* **2021**, *10* (1), 1940673.

(30) Zhou, W.; Hu, Z.; Wei, J.; Dai, H.; Chen, Y.; Liu, S.; Duan, Z.; Xie, F.; Zhang, W.; Guo, R. Quantum dots-hydrogel composites for biomedical applications. *Chin. Chem. Lett.* **2022**, *33* (3), 1245−1253.

(31) Varela-Fernández, R.; Bendicho-Lavilla, C.; Martin-Pastor, M.; Herrero Vanrell, R.; Lema-Gesto, M. I.; González-Barcia, M.; Otero-Espinar, F. J. Design, optimization, and in vitro characterization of idebenone-loaded PLGA microspheres for LHON treatment. *Int. J. Pharm.* **2022**, *616*, No. 121504.

(32) Asadi, N.; Annabi, N.; Mostafavi, E.; Anzabi, M.; Khalilov, R.; Saghfi, S.; Mehrizadeh, M.; Akbarzadeh, A. Synthesis, characterization and in vitro evaluation of magnetic nanoparticles modified with PCL-PEG-PCL for controlled delivery of 5FU. *Artif Cells Nanomed Biotechnol* **2018**, *46* (sup1), 938−945.

(33) Hao, J.; Fang, X.; Zhou, Y.; Wang, J.; Guo, F.; Li, F.; Peng, X. Development and optimization of solid lipid nanoparticle formulation for ophthalmic delivery of chloramphenicol using a Box-Behnken design. *Int. J. Nanomed.* **2011**, *6*, 683−92.

(34) Barabadi, H.; Honary, S.; Ebrahimi, P.; Alizadeh, A.; Naghibi, F.; Saravanan, M. Optimization of myco-synthesized silver nano-particles by response surface methodology employing Box-Behnken

design. *Synth. React. Inorg. Met.-Org. Nano-Met. Chem.* **2019**, *49*, 33−43.

(35) Qiao, J.; Li, X.; Qi, L. Fluorescent polymer-modified gold nanobipyramids for temperature sensing during photothermal therapy in living cells. *Chin. Chem. Lett.* **2022**, *33*, 3193 DOI: 10.1016/j.cclet.2021.12.070.

(36) Qiu, C.; Cheng, Z.; Lv, C.; Wang, R.; Yu, F. Development of bioorthogonal SERS imaging probe in biological and biomedical applications. *Chin. Chem. Lett.* **2021**, *32* (8), 2369−2379.

(37) Liao, J.; Pan, B.; Zhuo, X.; Liao, G.; Gao, Y.; Yao, Z.; Wang, L.; Wu, Q.; Pan, W.; Jiao, B.; Zhao, Q. *β*-1,2-Mannan-based glycoconjugates as potential antifungal vaccines. *Chin. Chem. Lett.* **2021**, *33*, 4345 DOI: 10.1016/j.cclet.2021.12.065.

(38) Goodarzi, H.; Jadidi, K.; Pourmotabed, S.; Sharifi, E.; Aghamollaei, H. Preparation and in vitro characterization of cross-linked collagen-gelatin hydrogel using EDC/NHS for corneal tissue engineering applications. *Int. J. Biol. Macromol.* **2019**, *126*, 620−632.

(39) Jiménez, R. A.; Millán, D.; Suesca, E.; Sosnik, A.; Fontanilla, M. R. Controlled release of an extract of Calendula officinalis flowers from a system based on the incorporation of gelatin-collagen microparticles into collagen I scaffolds: design and in vitro performance. *Drug Deliv Transl Res.* **2015**, *5* (3), 209−18.

(40) Tsekoura, E. K.; Dick, T.; Pankongadisak, P.; Graf, D.; Boluk, Y.; Uludağ, H. Delivery of Bioactive Gene Particles via Gelatin-Collagen-PEG-Based Electrospun Matrices. *Pharmaceuticals* **2021**, *14* (7), 666 DOI: 10.3390/ph14070666.

(41) Hsieh, C. M.; Yang, T. L.; Putri, A. D.; Chen, C. T. Application of Design of Experiments in the Development of Self-Micro-emulsifying Drug Delivery Systems. *Pharmaceuticals* **2023**, *16* (2), 283 DOI: 10.3390/ph16020283.

(42) Barabadi, H.; Honary, S.; Ebrahimi, P.; Alizadeh, A.; Naghibi, F.; Saravanan, M. Optimization of myco-synthesized silver nano-particles by response surface methodology employing Box-Behnken design. *Inorganic and Nano-Metal Chemistry* **2019**, *49* (2), 33−43.

(43) Varela-Fernández, R.; Bendicho-Lavilla, C.; Martin-Pastor, M.; Vanrell, R. H.; Lema-Gesto, M. I.; González-Barcia, M.; Otero-Espinar, F. J. Design, optimization, and in vitro characterization of idebenone-loaded PLGA microspheres for LHON treatment. *Int. J. Pharm.* **2022**, *616*, No. 121504.

(44) Pottathara, Y. B.; Kokol, V. Effect of nozzle diameter and cross-linking on the micro-structure, compressive and biodegradation properties of 3D printed gelatin/collagen/hydroxyapatite hydrogel. *Bioprinting* **2023**, *31*, No. e00266.

(45) Aghmiuni, A. I.; Baei, M. S.; Keshel, S. H.; Khiyavi, A. A. Design of novel 3D-scaffold as a potential material to induct epidermal-dermal keratinocytes of human-adipose-derived stem cells and promote fibroblast cells proliferation for skin regeneration. *Fibers Polym.* **2020**, *21*, 33−44.

(46) Su, X.; Chen, L.; Han, S.; Niu, G.; Ren, J.; Ke, C. Preparation and Characterization of a Novel Triple Composite Scaffold Containing Silk Fiborin, Chitosan, and Alginate for 3D Culture of Colonic Carcinoma Cells In Vitro. *Med. Sci. Monit.* **2020**, *26*, e922935.

(47) Hankiewicz, J.; Swierczek, E. Lysozyme in human body fluids. *Clin. Chim. Acta* **1974**, *57* (3), 205−9.

(48) Singh, Y. P.; Mishra, B.; Gupta, M. K.; Bhaskar, R.; Han, S. S.; Mishra, N. C.; Dasgupta, S. Gelatin/monetite electrospun scaffolds to regenerate bone tissue: Fabrication, characterization, and in-vitro evaluation. *Journal of the Mechanical Behavior of Biomedical Materials* **2023**, *137*, No. 105524.

(49) Tsao, C. J.; Pandolfi, L.; Wang, X.; Minardi, S.; Lupo, C.; Evangelopoulos, M.; Hendrickson, T.; Shi, A.; Storci, G.; Taraballi, F.; Tasciotti, E. Electrospun patch functionalized with nanoparticles allows for spatiotemporal release of VEGF and PDGF-BB promoting in vivo neovascularization. *ACS Appl. Mater. Interfaces* **2018**, *10* (51), 44344−44353.

(50) Liao, I. C.; Wan, A. C. A.; Yim, E. K. F.; Leong, K. W. Controlled release from fibers of polyelectrolyte complexes. *J. Controlled Release* **2005**, *104* (2), 347−358.

(51) Bunnell, B. A.; Flaat, M.; Gagliardi, C.; Patel, B.; Ripoll, C. Adipose-derived stem cells: isolation, expansion and differentiation. *Methods* **2008**, *45* (2), 115−20.

(52) Biagini, G.; Senegaglia, A. C.; Pereira, T.; Berti, L. F.; Marcon, B. H.; Stimamiglio, M. A. 3D Poly(Lactic Acid) Scaffolds Promote Different Behaviors on Endothelial Progenitors and Adipose-Derived Stromal Cells in Comparison With Standard 2D Cultures. *Front Bioeng Biotechnol* **2021**, *9*, No. 700862.

(53) Babaei, H.; Alibabrdel, M.; Asadian, S.; Siavashi, V.; Jabarpour, M.; Nassiri, S. M. Increased circulation mobilization of endothelial progenitor cells in preterm infants with retinopathy of prematurity. *Journal of Cellular Biochemistry* **2018**, *119* (8), 6575−6583.

(54) Jabarpour, M.; Siavashi, V.; Asadian, S.; Babaei, H.; Jafari, S. M.; Nassiri, S. M. Hyperbilirubinemia-induced pro-angiogenic activity of infantile endothelial progenitor cells. *Microvascular research* **2018**, *118*, 49−56.

(55) Siavashi, V.; Nassiri, S. M.; Rahbarghazi, R.; Vafaei, R.; Sariri, R. ECM-dependence of endothelial progenitor cell features. *Journal of cellular biochemistry* **2016**, *117* (8), 1934−1946.

(56) Méndez, V.; Avelar, E.; Morales, A.; Cervantes, M.; Araiza, A.; González, D. A rapid protocol for purification of total RNA for tissues collected from pigs at a slaughterhouse. *Genetics and molecular research: GMR* **2011**, *10* (4), 3251−3255.

(57) Tefas, L. R.; Tomuţă, I.; Achim, M.; Vlase, L. Development and optimization of quercetin-loaded PLGA nanoparticles by experimental design. *Clujul Med.* **2015**, *88* (2), 214−23.

(58) Dahmoune, F.; Spigno, G.; Moussi, K.; Remini, H.; Cherbal, A.; Madani, K. Pistacia lentiscus leaves as a source of phenolic compounds: Microwave-assisted extraction optimized and compared with ultrasound-assisted and conventional solvent extraction. *Industrial Crops and Products* **2014**, *61*, 31−40.

(59) Feng, R.; Song, Z.; Zhai, G. Preparation and in vivo pharmacokinetics of curcumin-loaded PCL-PEG-PCL triblock co-polymeric nanoparticles. *Int. J. Nanomedicine* **2012**, *7*, 4089−98.

(60) Danafar, H. Preparation and characterization of PCL-PEG-PCL polymersomes for delivery of clavulanic acid. *Cogent Medicine* **2016**, *3* (1), 1235245.

(61) De Meutter, J.; Goormaghtigh, E. Amino acid side chain contribution to protein FTIR spectra: impact on secondary structure evaluation. *Eur. Biophys. J.* **2021**, *50*, 641−651.

(62) Huynh, D. P.; Nguyen, M. K.; Kim, B. S.; Lee, D. S. Molecular design of novel pH/temperature-sensitive hydrogels. *Polymer* **2009**, *50* (12), 2565−2571.

(63) Fu, S. Z.; Wang, X. H.; Guo, G.; Shi, S.; Fan, M.; Liang, H.; Luo, F.; Qian, Z. Y. Preparation and properties of nano-hydroxyapatite/PCL-PEG-PCL composite membranes for tissue engineering applications. *J. Biomed. Mater. Res. Part B* **2011**, *97* (1), 74−83.

(64) Cui, Y.; Jin, R.; Zhou, Y.; Yu, M.; Ling, Y.; Wang, L. Q. Crystallization enhanced thermal-sensitive hydrogels of PCL-PEG-PCL triblock copolymer for 3D printing. *Biomed. Mater.* **2021**, *16* (3), No. 035006. DOI: 10.1088/1748-605X/abc38e.

(65) Vassallo, V.; Tsianaka, A.; Alessio, N.; Grübel, J.; Cammarota, M.; Tovar, G. E.; Southan, A.; Schiraldi, C. Evaluation of novel biomaterials for cartilage regeneration based on gelatin methacryloyl interpenetrated with extractive chondroitin sulfate or unsulfated biotechnological chondroitin. *J. Biomed. Mater. Res., Part A* **2022**, *110* (6), 1210−1223.

(66) Waldner, M.; Zhang, W.; James, I. B.; Allbright, K.; Havis, E.; Bliley, J. M.; Almadori, A.; Schweizer, R.; Plock, J. A.; Washington, K. M.; Gorantla, V. S.; Solari, M. G.; Marra, K. G.; Rubin, J. P. Characteristics and Immunomodulating Functions of Adipose-Derived and Bone Marrow-Derived Mesenchymal Stem Cells Across Defined Human Leukocyte Antigen Barriers. *Front. Immunol.* **2018**, *9*, 1642.

(67) Ito, R.; Morimoto, N.; Pham, L. H.; Taira, T.; Kawai, K.; Suzuki, S. Efficacy of the controlled release of concentrated platelet lysate from a collagen/gelatin scaffold for dermis-like tissue

regeneration. *Tissue Engineering Part A* **2013**, *19* (11−12), 1398−1405.

(68) Redmond, J.; McCarthy, H. O.; Buchanan, P.; Levingstone, T. J.; Dunne, N. J. Development and characterisation of 3D collagen-gelatin based scaffolds for breast cancer research. *Biomaterials Advances* **2022**, *142*, No. 213157.

(69) Guo, Y.; Huang, J.; Fang, Y.; Huang, H.; Wu, J. 1D, 2D, and 3D scaffolds promoting angiogenesis for enhanced wound healing. *Chem. Eng. J.* **2022**, *437*, No. 134690. DOI: 10.1016/j.cej.2022.134690.

(70) Song, S.; Liu, X.; Huang, J.; Zhang, Z. Neural stem cell-laden 3D bioprinting of polyphenol-doped electroconductive hydrogel scaffolds for enhanced neuronal differentiation. *Biomaterials Advances* **2022**, *133*, No. 112639.

(71) Pitrolino, K. A.; Felfel, R. M.; Pellizzeri, L. M.; McLaren, J.; Popov, A. A.; Sottile, V.; Scotchford, C. A.; Scammell, B. E.; Roberts, G. A.; Grant, D. M. Development and in vitro assessment of a bi-layered chitosan-nano-hydroxyapatite osteochondral scaffold. *Carbohydr. Polym.* **2022**, *282*, No. 119126.

(72) Grzybek, P.; Jakubski, Ł.; Dudek, G. Neat Chitosan Porous Materials: A Review of Preparation, Structure Characterization and Application. *International Journal of Molecular Sciences* **2022**, *23* (17), 9932.

(73) Du, X.; Dehghani, M.; Alsaadi, N.; Nejad, M. G.; Saber-Samandari, S.; Toghraie, D.; Su, C.-H.; Nguyen, H. C. A femoral shape porous scaffold bio-nanocomposite fabricated using 3D printing and freeze-drying technique for orthopedic application. *Mater. Chem. Phys.* **2022**, *275*, No. 125302.

(74) Davidenko, N.; Schuster, C. F.; Bax, D. V.; Farndale, R. W.; Hamaia, S.; Best, S. M.; Cameron, R. E. Evaluation of cell binding to collagen and gelatin: a study of the effect of 2D and 3D architecture and surface chemistry. *J. Mater. Sci. Mater. Med.* **2016**, *27* (10), 148.

(75) Agache, P. G.; Monneur, C.; Leveque, J. L.; De Rigal, J. Mechanical properties and Young's modulus of human skin in vivo. *Archives of Dermatological Research* **1980**, *269* (3), 221−232.

(76) Zhou, L.; Zeng, Z.; Liu, S.; Min, T.; Zhang, W.; Bian, X.; Du, H.; Zhang, P.; Wen, Y. Multifunctional DNA Hydrogel Enhances Stemness of Adipose-Derived Stem Cells to Activate Immune Pathways for Guidance Burn Wound Regeneration. *Adv. Funct. Mater.* **2022**, *32* (46), 2207466.

(77) Nokoorani, Y. D.; Shamloo, A.; Bahadoran, M.; Moravvej, H. Fabrication and characterization of scaffolds containing different amounts of allantoin for skin tissue engineering. *Sci. Rep.* **2021**, *11* (1), 16164.

(78) Ampawong, S.; Aramwit, P. A study of long-term stability and antimicrobial activity of chlorhexidine, polyhexamethylene biguanide, and silver nanoparticle incorporated in sericin-based wound dressing. *J. Biomater Sci. Polym. Ed* **2017**, *28* (13), 1286−1302.

(79) Lakra, R.; Kiran, M. S.; Sai Korrapati, P. Collagen scaffold reinforced with furfural for wound healing application. *Mater. Lett.* **2022**, *315*, No. 131956.

(80) Van Liedekerke, P.; Gannoun, L.; Loriot, A.; Johann, T.; Lemaigre, F. P.; Drasdo, D. Quantitative modeling identifies critical cell mechanics driving bile duct lumen formation. *PLOS Computational Biology* **2022**, *18* (2), No. e1009653.

(81) Lv, H.; Li, L.; Sun, M.; Zhang, Y.; Chen, L.; Rong, Y.; Li, Y. Mechanism of regulation of stem cell differentiation by matrix stiffness. *Stem Cell Res. Ther.* **2015**, *6* (1), 1−11.

(82) Fard, M.; Akhavan-Tavakoli, M.; Khanjani, S.; Zare, S.; Edalatkhah, H.; Arasteh, S.; Mehrabani, D.; Zarnani, A.-H.; Kazemnejad, S.; Shirazi, R. Bilayer amniotic membrane/nano-fibrous fibroin scaffold promotes differentiation capability of menstrual blood stem cells into keratinocyte-like cells. *Molecular biotechnology* **2018**, *60*, 100−110.

(83) Li, M.; Ma, J.; Gao, Y.; Dong, M.; Zheng, Z.; Li, Y.; Tan, R.; She, Z.; Yang, L. Epithelial differentiation of human adipose-derived stem cells (hASCs) undergoing three-dimensional (3D) cultivation with collagen sponge scaffold (CSS) via an indirect co-culture strategy. *Stem Cell Res. Ther.* **2020**, *11* (1), 141.

(84) Staji, M.; Sadeghzadeh, N.; Zamanlui, S.; Azarani, M.; Golchin, A.; Soleimani, M.; Ardeshirylajimi, A.; Khojasteh, A.; Hosseinzadeh, S. Evaluation of dermal growth of keratinocytes derived from foreskin in co-culture condition with mesenchymal stem cells on polyurethane/gelatin/amnion scaffold. *International Journal of Polymeric Materials and Polymeric Biomaterials* **2023**, *72* (5), 386−396.

(85) Lotfi, Z.; Khakbiz, M.; Davari, N.; Bonakdar, S.; Mohammadi, J.; Shokrgozar, M. A.; Derhambakhsh, S. Fabrication and multiscale modeling of polycaprolactone/amniotic membrane electrospun nano-fiber scaffolds for wound healing. *Artif Organs* **2023**, *47* (8), 1267−1284.

(86) Ghiasi, M.; Hashemi, M.; Salimi, A.; Jadidi, K.; Tavallaie, M.; Aghamollaei, H. Combination of natural scaffolds and conditional medium to induce the differentiation of adipose-derived mesenchymal stem cells into keratocyte-like cells and its safety evaluation in the animal cornea. *Tissue and Cell* **2023**, *82*, No. 102117.

(87) Naomi, R.; Bahari, H.; Ridzuan, P. M.; Othman, F. Natural-based biomaterial for skin wound healing (Gelatin vs. collagen): Expert review. *Polymers* **2021**, *13* (14), 2319.

(88) Mousavi, S.; Khoshfetrat, A. B.; Khatami, N.; Ahmadian, M.; Rahbarghazi, R. Comparative study of collagen and gelatin in chitosan-based hydrogels for effective wound dressing: Physical properties and fibroblastic cell behavior. *Biochem. Biophys. Res. Commun.* **2019**, *518* (4), 625−631.

(89) Huang, J.; Lei, X.; Huang, Z.; Rong, Z.; Li, H.; Xie, Y.; Duan, L.; Xiong, J.; Wang, D.; Zhu, S. Bioprinted Gelatin-Recombinant Type III Collagen Hydrogel Promotes Wound Healing. *Int. J. Bioprint.* **2022**, *8* (2), 517 DOI: 10.18063/ijb.v8i2.517.

(90) Santhini, E.; Parthasarathy, R.; Shalini, M.; Dhivya, S.; Mary, L. A.; Padma, V. V. Bio inspired growth factor loaded self assembling peptide nano hydrogel for chronic wound healing. *Int. J. Biol. Macromol.* **2022**, *197*, 77−87.

(91) Soontornworajit, B.; Zhou, J.; Shaw, M. T.; Fan, T.-H.; Wang, Y. Hydrogel functionalization with DNA aptamers for sustained PDGF-BB release. *Chem. Commun.* **2010**, *46* (11), 1857−1859.

(92) Thomopoulos, S.; Zaegel, M.; Das, R.; Harwood, F. L.; Silva, M. J.; Amiel, D.; Sakiyama-Elbert, S.; Gelberman, R. H. PDGF-BB released in tendon repair using a novel delivery system promotes cell proliferation and collagen remodeling. *Journal of Orthopaedic Research* **2007**, *25* (10), 1358−1368.

(93) Lee, J.; Yoo, J. J.; Atala, A.; Lee, S. J. The effect of controlled release of PDGF-BB from heparin-conjugated electrospun PCL/gelatin scaffolds on cellular bioactivity and infiltration. *Biomaterials* **2012**, *33* (28), 6709−6720.

(94) Li, Y.; Liu, Z.; Zhao, C.; Xu, C.; Shin, A.; Wu, J.; Li, D.; Lin, K.; Liu, J. A sustained-release PDGF-BB nanocomposite hydrogel for DM-associated bone regeneration. *J. Mater. Chem. B* **2023**, *11*, 974−984.

(95) Wei, G.; Jin, Q.; Giannobile, W. V.; Ma, P. X. Nano-fibrous scaffold for controlled delivery of recombinant human PDGF-BB. *J. Controlled Release* **2006**, *112* (1), 103−110.

(96) Petry, L.; Kippenberger, S.; Meissner, M.; Kleemann, J.; Kaufmann, R.; Rieger, U. M.; Wellenbrock, S.; Reichenbach, G.; Zöller, N.; Valesky, E. Directing adipose-derived stem cells into keratinocyte-like cells: impact of medium composition and culture condition. *J. Eur. Acad. Dermatol Venereol* **2018**, *32* (11), 2010−2019.

(97) Xie, F.; Tang, X.; Zhang, Q.; Deng, C. Reprogramming human adipose tissue stem cells using epidermal keratinocyte extracts. *Mol. Med. Rep* **2015**, *11* (1), 182−8.

(98) Edwards, N. J.; Stone, R.; Christy, R.; Zhang, C. K.; Pollok, B.; Cheng, X. Differentiation of adipose derived stem cells to keratinocyte-like cells on an advanced collagen wound matrix. *Tissue Cell* **2018**, *53*, 68−75.

(99) Kim, J.; Hasegawa, T.; Wada, A.; Maeda, Y.; Ikeda, S. Keratinocyte-Like Cells Trans-Differentiated from Human Adipose-Derived Stem Cells, Facilitate Skin Wound Healing in Mice. *Ann. Dermatol* **2021**, *33* (4), 324−332.

(100) Natesan, S.; Wrice, N. L.; Christy, R. J. Peroxisome proliferator-activated receptor-α agonist and all-trans retinoic acid

induce epithelial differentiation of subcutaneous adipose-derived stem cells from debrided burn skin. *J. Cell Biochem* **2019**, *120* (6), 9213−9229.

(101) Brzoska, M.; Geiger, H.; Gauer, S.; Baer, P. Epithelial differentiation of human adipose tissue-derived adult stem cells. *Biochem. Biophys. Res. Commun.* **2005**, *330* (1), 142−50.

(102) Alizadeh, E.; Zarghami, N.; Eslaminejad, M. B.; Akbarzadeh, A.; Barzegar, A.; Mohammadi, S. A. The effect of dimethyl sulfoxide on hepatic differentiation of mesenchymal stem cells. *Artificial Cells, Nanomedicine, and Biotechnology* **2016**, *44* (1), 157−164.

(103) Yi, J. K.; Park, S.; Ha, J. J.; Kim, D. H.; Huang, H.; Park, S. J.; Lee, M. H.; Ryoo, Z. Y.; Kim, S. H.; Kim, M. O. Effects of Dimethyl Sulfoxide on the Pluripotency and Differentiation Capacity of Mouse Embryonic Stem Cells. *Cell Reprogram* **2020**, *22* (5), 244−253.